

Prageeth Jayathissa

Design and Assessment of Adaptive Photovoltaic Envelopes



PRAGEETH JAYATHISSA

DESIGN AND ASSESSMENT OF ADAPTIVE
PHOTOVOLTAIC ENVELOPES

DISS. ETH NO. ?

DESIGN AND ASSESSMENT OF ADAPTIVE PHOTOVOLTAIC ENVELOPES

A dissertation submitted to attain the degree of

DOCTOR OF SCIENCES of ETH ZURICH
(Dr. sc. ETH Zurich)

presented by

PRAGEETH JAYATHISSA
Msc., ETH Zurich

born on 27 September 1988
citizen of New Zealand

accepted on the recommendation of

Prof. Dr. A. Schlueter, examiner
Prof. Dr. Z. Nagy, co-examiner

2017

Prageeth Jayathissa: *Design and Assessment of Adaptive Photovoltaic Envelopes*,
© 2017

DOI: 10.3929/ethz-a-

To Someone

ABSTRACT

Adaptive photovoltaic envelopes have the potential to improve building energy performance by controlling natural lighting and solar heat gains, while simultaneously generating electricity to match the building demand. This study analyses the potential of adaptive photovoltaic envelopes, from the design process to its evaluation. The study first presents a performative design environment that combines multiple technological branches into a single automated workflow. The environment designs the form of the facade, provides feedback on its structural strength, analyses the energetic performance of the interior space, conducts a daylighting analysis, renders images and produces fabrication plans for a rapid design process. Through this methodology an adaptive photovoltaic envelope known as the Adaptive Solar Facade was successfully designed and constructed. The control strategy for the adaptive envelope is built using a model predictive control algorithm which runs successive simulations of the electricity production and building energy demand for all possible angle configurations of the panels. Angle configurations that result in minimum building energy demand, sufficient daylighting, and maximum electricity production are chosen. This control strategy can also be numerically evaluated over a year and results show that an adaptive system can have a 20% - 80% energy saving over an equivalent static system. The large range is due to the sensitivity of the building type. Running this numerical evaluation over eleven building use types spanning six construction periods show that modern offices, schools, and retail stores are ideal application cases. The adaptive envelopes ultimately perform best when there is a mix of both heating and cooling demands in the building space. A CO₂ life cycle analysis of the adaptive solar facade shows that it is favourably competitive to traditional building integrated photovoltaic systems.

ZUSAMMENFASSUNG

Deutsche Zusammenfassung hier.

ACKNOWLEDGEMENTS

I would like to thank my team: Bratislav Svetozarevic, Moritz Begle and Stefan Caranovic. Through all the late nights, near impossible problems, and moments of genius we managed to get this technology working. I would also like to thank my students that played an important role in this thesis. In particular Nico Offeddu, Michale Jansen, Jerimias Schmidli, Maruo Luzzatto, Justin Zarb, and Stefan Caranovic (yes Stefan, you were mentioned twice...)

I would then like to thank my direct supervisors. Arno Schlueter for supervising my research throughout my PhD, Zoltan Nagy for getting me started through the complications of the first year and continuing to support as my co-supervisor till the end, and Johannes Hofer for being a mentor through the end stages of my work.

Next on the list come the rest of the A/S Team. In particular I would like to thank Daren Thomas for his support in software development and general fun, Mario Frei for his electronics support and German language proof reading, Jimeno Fonseca for supervising me in the first weeks and introducing me to the world of building engineering, Clayton Miller for his python support, Anja Willmann for supporting with architectural aspects of the design, and Geroid Lydon for managing the HiLo development. I would also like to extend this thank you to Amr Elesawy, Illias Hischer, Martin Mosteiro Romero, Hu Zhao for their inspiration and always there for a coffee or beer break. From the Singapore team, I would like to thank Gabriel Happle and Shan-Shan Hsieh for supporting me in the development of the RC Model. I would like to also thank Niko Herren for supporting me in life cycle assessments.

I would like to extend this thank you to the HiLo and HoNR project members for the design and construction of the ASF: Supermanoeuvre (Sydney Australia) and the Professorship of Architecture and Structures (BRG, ETH Zurich) for their work in designing the HiLo building; and the Institute of Structural Engineering (IBK, ETH Zurich) for their work in designing the HoNR building. In particular, I would like to thank Dave Pigram for leading the architectural integration of the ASF to HiLo.

Finally, I would like to thank my friends and family for always being there for me.

CONTENTS

1	INTRODUCTION	1
1.1	Research Questions	3
1.2	Organisation of the Thesis	5
2	PARAMETRIC DESIGN ENVIRONMENT FOR KINETIC PHOTO-VOLTAIC ARCHITECTURE	7
2.1	Introduction	8
2.2	Methodology	10
2.2.1	Structural form finding and finite element analysis	11
2.2.2	Energy Evaluation	13
2.2.3	Integration of classical design methods	15
2.3	Case Study	16
2.3.1	Optimum PV Panel Layout	16
2.3.2	Structure	17
2.3.3	Structural Validation	18
2.3.4	Module Design	20
2.3.5	Fabrication	21
2.4	Discussion and Conclusion	21
3	OPTIMISING BUILDING NET ENERGY DEMAND WITH DYNAMIC BIPV SHADING	27
3.1	Introduction	28
3.2	Methodology	30
3.2.1	Radiation Analysis	31
3.2.2	PV Circuit Simulation	31
3.2.3	RC Model for Building Energy Demand	33
3.2.4	Lighting Model	35
3.2.5	Exhaustive Search Optimisation	36
3.2.6	Case Study	36
3.3	Results	36
3.3.1	Daily Energetic and Control Profiles of the ASF	38
3.3.2	Optimum Annual Configurations	39
3.3.3	Comparison With Other Systems	43
3.4	Discussion	44
3.5	Conclusion	47

4	SENSITIVITY OF BUILDING PROPERTIES AND USE TYPES FOR THE APPLICATION OF ADAPTIVE PHOTOVOLTAIC SHADING SYSTEMS	49
4.1	Introduction	50
4.2	Methodology	51
4.2.1	Sensitivity Analysis	52
4.2.2	Analysis of Archetypes	52
4.3	Results	53
4.3.1	Sensitivity of the Building Envelope	53
4.3.2	Archetype Evaluation of the ASF	56
4.4	Discussion and Conclusion	57
5	LIFE CYCLE ASSESSMENT OF DYNAMIC BUILDING INTEGRATED PHOTOVOLTAICS	59
5.1	Introduction	60
5.2	Methodology	62
5.2.1	Embodied Life Cycle Inventory	64
5.2.2	Operational Life Cycle Inventory	68
5.2.3	Sensitivity Analysis	70
5.3	Results	71
5.3.1	LCA of the Adaptive Solar Facade Manufacture	71
5.3.2	Calculation of GWP Emission Factor	72
5.3.3	Sensitivity Analysis	73
5.3.4	Comparison to existing PV technologies	75
5.4	Discussion	76
5.5	Conclusion	78
6	CONCLUSION	81
6.1	Outlook	82
A	APPENDIX	83
A.1	Full Set of Equations to the Building Model	83
A.2	LCA Parameters	84
A.2.1	Electricity production of different PV Systems	84
A.2.2	Major Contributions to Disposal	86
	BIBLIOGRAPHY	89

NOTATION

FREQUENTLY USED SYMBOLS

T_e	Outdoor air temperature °C
T_m	Thermal mass temperature °C
T_s	Internal wall surface temperature °C
T_{air}	Indoor air temperature °C
T_{sup}	Ventilation supply air temperature °C
H_{em}	Wall thermal conductance W/K
H_{ms}	Internal conductance between the internal surface and mass W/K
H_{is}	Internal conductance between the indoor air and internal surface W/K
H_{ve}	Ventilation thermal conductance W/K
H_w	Window thermal conductance W/K
H_{tr}	Equivalent thermal conductance, see Appendix W/K
C_m	Thermal Capacitance J/K
ϕ_{HC}	Heating or cooling load W
ϕ_{sol}	Solar heat gain W
ϕ_{int}	Internal heat gain W
ϕ_{mtot}	Equivalent heat flux, see Appendix W
φ_{flux}	Luminance per floor area Lx
E_w	Incident luminance on the window Lumens
G	Solar transmittance of the window
M	Maintenance factor of the window
U	Utilisation factor of the window
ACH	Air Changes per Hour
V_{room}	Volume of a room

ABBREVIATIONS

ASF	Adaptive Solar Facade
-----	-----------------------

PDE	Performative Design Environment
BIM	Building Information Modelling
FEA	Finite Element Analysis
BIPV	Building Integrated Photovoltaic
PV	Photovoltaic
HVAC	Heating Ventilation and Air Conditioning
CIGS	Copper Indium Gallium Selenide
CdTe	Cadmium Telluride
COP	Coefficient of Performance
CEA	City Energy Analyst
LCA	Life Cycle Analysis
SMQ	Specific Mass Quantity
GWP	Global Warming Potential

(CODATA 2014 [1])

INTRODUCTION

Intelligence is the ability to adapt to change

— Stephen Hawkin

A building, in its original manifestation, is a shelter. A means to protect the human body from harsh external conditions. And within this we ascribe the notion of the envelope, the barrier between the external and internal environments. It is the barrier that protects us from frigid temperatures, shades us from solar rays, and keeps us dry when a storm passes by. And over time, we have not just developed the quality of our envelopes, but also technologies that enable us to manufacture interior environments. The combination of heating, cooling, lighting and air handling enables us to exclude the energies of the exterior and form hermetic envelopes. Buildings transformed from mere shelters, to places of comfort where we now spend 87% of our lives [2]. We have in essence, become an indoor species.

Unfortunately, the manufacture of interior environments comes with a large environmental impact. Buildings are currently responsible for 32% of our final energy use and 19% of our total greenhouse gas emissions [3]. There is, however, a 50% - 90% emission reduction potential using existing technologies [3]. On one hand, the efficiency of our manufactured interior environment can be increased. We can install more efficient systems to manufacture this energy at a lower environmental cost. We can further increase the isolation properties of our envelopes, thus reducing the energetic loss to the exterior. On the other hand, we can rewind the clock of architectural history and move back to a time where we did not manufacture internal environments, but rather mediated the external energies to fulfil that of the interior. These strategies, commonly described as passive design strategies, include aspects such as natural ventilation, thermal storage, and static shading.

Instead of rewinding the clock of architectural history, there is also the possibility to look ahead. With new technologies the mediation of the external environment is not restricted to passive strategies, but also active ones. The mediation of solar radiation through responsive shading is one such example. A responsive shading system will open when solar radiation levels are low to maximise natural lighting, and close when the radiation

reaches a critical peak at which the building begins to overheat. Iconic examples include the Al Bahr Towers in Dubai [4], the Arab World Institute in Paris, and the ThyssenKrupp Headquarters in Essen.

In an ideal setting, as shown in Figure 1.1, the envelope does not just exist in an open or closed state, but in a multitude of states fulfilling various functions. The modularity described in this schematic enables certain parts of the envelope to respond for optimal daylight distribution, whereas others are optimised for heating / cooling demand reduction, and enhancing views to the exterior. If we also replace the envelope material with light weight thin film solar panels, we can also harvest solar energy onsite and use it to meet the demands of the interior space. It is through this modularity that we can best balance user comfort, with building energy saving.

This modularity however introduces new challenges in terms of control. In a responsive system the designer sets threshold radiation levels at which the envelope opens and closes. This modular envelope however, can have thousands of possible states, and needs to find the optimum balance between building energy demand reduction, occupant comfort, and PV electricity production. It is in this context that I coin the term adaptive. An adaptive envelope senses its environment, such as the occupancy, interior temperature, exterior temperature and radiation levels, and then determines the optimum envelope configuration to mediate a comfortable interior environment while minimising the total net energy consumption.

This adaptive nature can span different time durations. In the short time span, if the sun goes behind a cloud, or the occupancy dramatically increases, the envelope will be able to adapt to meet this new environment. Likewise, the envelope will also adapt to long term variations such as global warming.

This dissertation is written in the context of the Adaptive Solar Facade (ASF), an adaptive photovoltaic envelope designed for a research and innovation unit known as the HiLo [5]. The ASF is a modular facade of 40 x 40 cm copper indium gallium selenide (CIGS) PV panels that can be actuated in two degrees of freedom with a range of 90°. An example of this, mounted on a testing site can be seen in Figure 1.2.

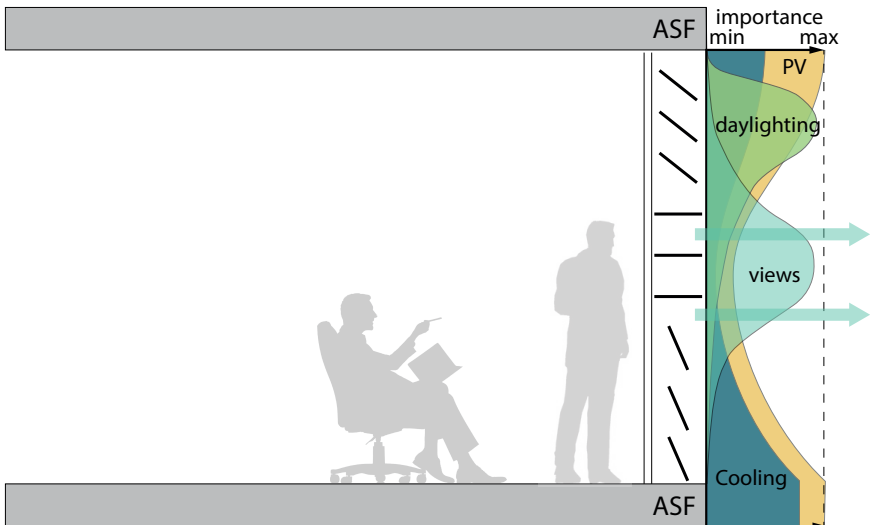


FIGURE 1.1: A modular facade adptive to various functions for optimising occupant comfort

1.1 RESEARCH QUESTIONS

The four questions addressed in this research are

- How can complex architectural components, such as the ASF be designed and constructed?
- How can a photovoltaic envelope be controlled to be adaptive?
- What is the energy saving potential of an adaptive photovoltaic envelope?
- How does the energy saving potential vary for different building types?
- What is the life cycle CO₂ saving potential of an adaptive photovoltaic facade?

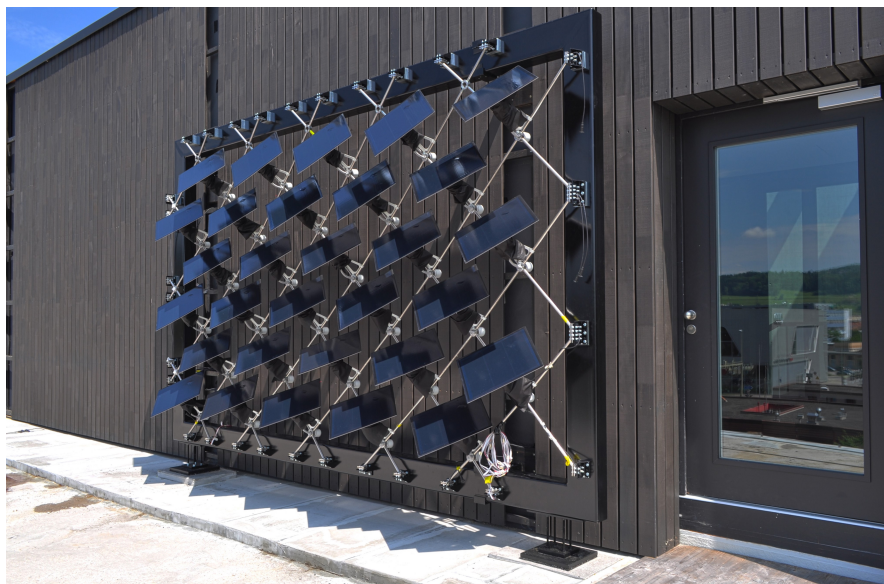


FIGURE 1.2: The final Adaptive Solar Facade, mounted on a testing site prior to assembly on the HiLo Module

1.2 ORGANISATION OF THE THESIS

The remainder of this thesis is composed of three journal papers and one conference paper. Chapter 2 introduces the parametric design environment, which was created for rapid iterative development of the ASF. This chapter also introduces some of the design elements of the ASF. Chapter 3 introduces the model predictive control strategy to allows for adaptive control. This chapter first introduces the simulation methodology, and then discusses the energy saving potential of an ASF system. Chapter 4 takes on the model from Chapter 3 and runs an evaluation on eleven different building use types spanning six construction periods. Chapter 5 then takes the results of the energy simulation methodology and assesses the carbon life cycle cost. Finally Chapter 6 concludes the thesis.

2

PARAMETRIC DESIGN ENVIRONMENT FOR KINETIC PHOTOVOLTAIC ARCHITECTURE

Performative design environments can accelerate the design process by integrating multiple technological branches into a unified platform. This paper presents a performative design environment that combines the branches of structural and energy engineering, control, industrial design, and architecture. The methodology is applied in the context of the Adaptive Solar Facade, a kinetic photovoltaic shading system for the HiLo building in Duebendorf, Switzerland. We describe how the environment enables the user to design the form of the facade, get feedback on its structural strength, analyse the energetic performance of the interior space, conduct a daylighting analysis, render images, and produce fabrication plans for a rapid design process. With the design environment, project meetings transform from information exchanges to design sessions where all stakeholders can collaboratively influence the design and see immediate results. What would normally take a month, was condensed to just a few hours. Ultimately, we show how a system as complex as a kinetic photovoltaic envelope can be designed, prototyped, and fabricated by a small team of four designers.

2.1 INTRODUCTION

The interest for applying kinetic envelopes in architecture has increased in recent years. On one hand, there is the availability of digital design processes, which enables kinetic concepts to come to life. On the other hand, there is the desire to have active building elements to regulate energy flows to create a more sustainable built environment [6].

When analysing the various energy flows, it is solar radiation that is of particular interest. As seen in Figure 2.1 the mediation of solar radiation has the potential to reduce heating and cooling demands, while simultaneously distributing daylight according to the occupants' desires [7]. Furthermore, utilising thin film photovoltaic panels as the kinetic element enables the facade to also act as an electricity generator. It has been shown that such technologies can, in some cases, offset the entire energy consumption of the building space behind the envelope [8].

The application of kinetic architectural envelopes has so far been centred around iconic examples. These include the Al Bahr Towers in Dubai [4], the Arab World Institute in Paris, and the ThyssenKrupp Headquarters in Essen. Bringing these technologies to the mainstream, however, can be challenging.

One major challenge in the design of Kinetic Architectural Elements is the involvement of multiple technological branches. Among these branches we can count structural and energy engineering, control, industrial design, and architecture. Each of these branches has strong interdependencies to each other. For example, during the detail design process, a small variation in the control system such as the range of movement can affect energetic performance and architectural image. This may result in a redesign, that then needs to undergo structural evaluations and fit within the budget. These iteration cycles become a time intensive process that, in some cases, can take months to solve. In order to unite these branches efficiently, new design methods and environments have to be developed.

The state of the art in interdisciplinary building design lies in building information modelling (BIM) [9, 10]. The utilisation of BIM to perform fast energy and structural assessments enables an integrated design from the early design stages. However, the design is often based on high levels of standardisation, which makes it complicated when designing custom innovative components. The development of kinetic architectural envelopes

requires a flexible infrastructure, which allows for fast design, prototyping and production, while maintaining the ability to be customized for each system individually.

One way of overcoming these limitations of BIM is through performative design [11]. Performative design takes computer aided design (CAD) in a reversed manner, where it is the simulations that drive the design. Here, the concept of form making, is replaced with form finding. An example of performative design has been described by Turrin et al. where passive solar strategies were explored to improve the thermal comfort and daylight quality under a tessellated roof [12]. This can also stretch to structural performative design in tools such as RhinoVault where the final form is determined through iterative structural simulations [13]. Holzer on the other hand used performative design for direct structural feedback using first and second order structural simulations [14]. These tools can also be utilised on the component level, and have been previously analysed in a design studio for smart building envelopes [15]. However, integrating multiple tools in a single automated environment has still proven to be difficult due to some tools lacking parametrisation capabilities, low openness of the tools interfaces, and low flexibility [16, 17].

In this paper, we build on this existing knowledge to produce a state of the art performative design environment (PDE) that can shape the form of a facade, provide feedback on its structural strength, analyse the energetic performance and day-lighting conditions of the building space, render images, and produce fabrication drawings for a rapid iterative design process. This is accomplished within the Rhino/Grasshopper environment with python as a scripting language. The methodology is applied in the context of the Adaptive Solar Facade (ASF), a kinetic photovoltaic facade constructed for a research and innovation unit known as the HiLo [5]. HiLo is a two bedroom apartment with a portfolio of energy saving technologies that create a net zero energy building [18]. Both bedrooms of the HiLo will be equipped with an ASF as seen in Figure 2.2. The adaptive control of solar radiation into the bedrooms, coupled with on site electricity generation will contribute to this overall net zero energy strategy. We will present the entire design process from conceptual design, to prototyping, and final fabrication.

The remainder of the paper is organised as follows: the next section details the parametric design environment and the simulations that drive the final design, in Section 2.3 we describe the outcomes of this design

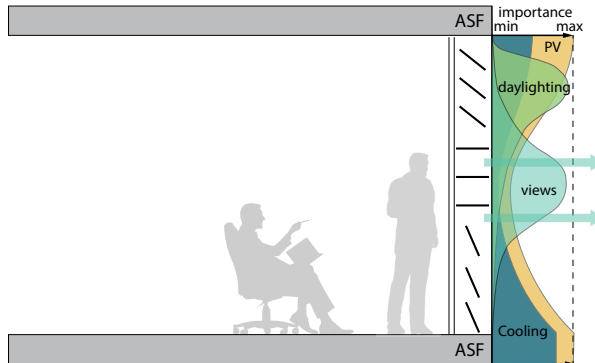


FIGURE 2.1: The facade acting as a mediator between the interior and exterior environment, while fulfilling various functions [7]

process including the details of the kinetic facade, and in Section 2.4 we discuss the limitations of this environment and conclude the paper.

2.2 METHODOLOGY

The parametric design environment (PDE), shown schematically in Figure 2.3 details the multiple processes that were used in parallel to handle the different technological branches. From this, four key outputs are generated: the structural performance, energetic performance, manufacturing plans, and visual renders. Inputs to the PDE are defined by the parameters that have the greatest influence on the design. In this case, they are the overall frame dimension and profile, the photovoltaic panel dimension, spacing and layout, and the range of motion. These inputs are numerically fed into the design environment and generate instantaneous results, allowing for quick feedback loops with the major stakeholders (architects, structural engineering, energy engineers, and production team) involved in the project.

The environment combines the geometric modelling software Rhinoceros 3D [19], its parametric plug-in Grasshopper [20], and python [21] as a scripting language. The relatively unspecialised nature of Rhino is complemented by a large number of specialised add-ons for Grasshopper. Furthermore, custom Grasshopper modules can be scripted using python. The

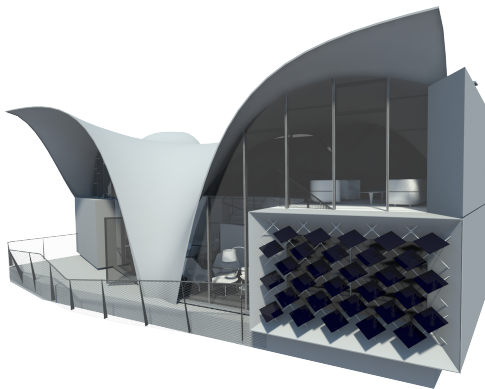


FIGURE 2.2: Render of the HiLo module to be constructed in Dubendorf, Switzerland. Two adaptive solar facades have been planned on the south and west facing facades.

following subsections will explain the structural and energetic analysis in more detail.

2.2.1 *Structural form finding and finite element analysis*

The proposed ASF is based on a vaulted cross-hatched network of stainless steel pipes as seen in Figure 2.4. The junctions where the pipes cross serve as the mounting points for each dynamic photovoltaic module. All utility lines are routed within the pipe network. A steel frame supports the pipe network to create a stand-alone pre fabricated component, which can be mounted directly to the building envelope. The vaulted shape further strengthens the structure against wind loads, thus allowing for thinner pipe diameters, which increases transparency.

The form of the vaulted structure is determined through RhinoVault, a form finding plug in for Grasshopper [13]. The method calculates the optimum shape of the pipe network based on the loading points and inputs to the design environment. Once the form is determined, a structural second order finite element analysis is conducted using the Karamba3d plug-in [22] to dimension the structural elements. Further manual adjust-

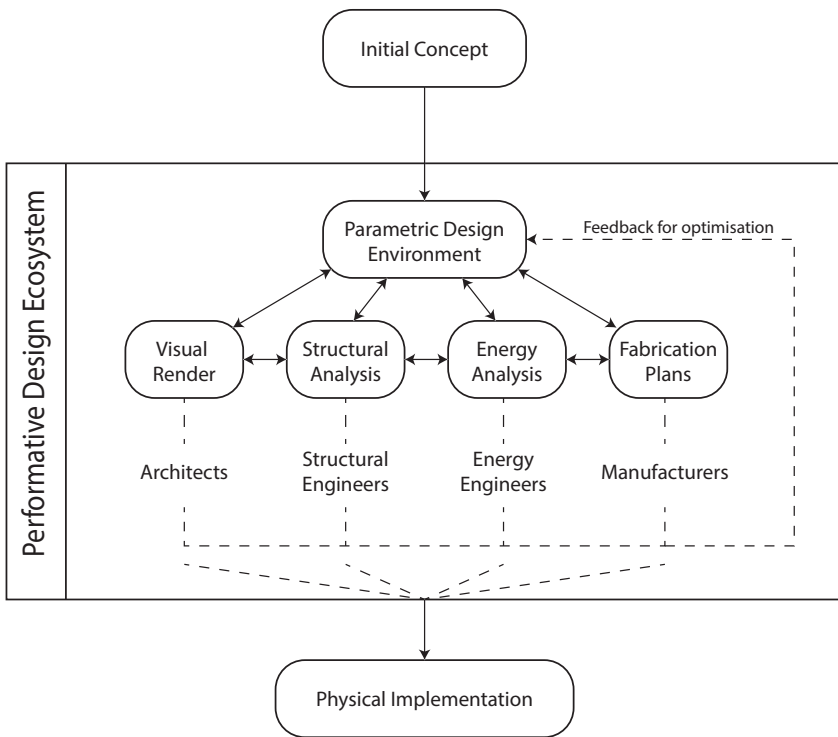


FIGURE 2.3: The PDE

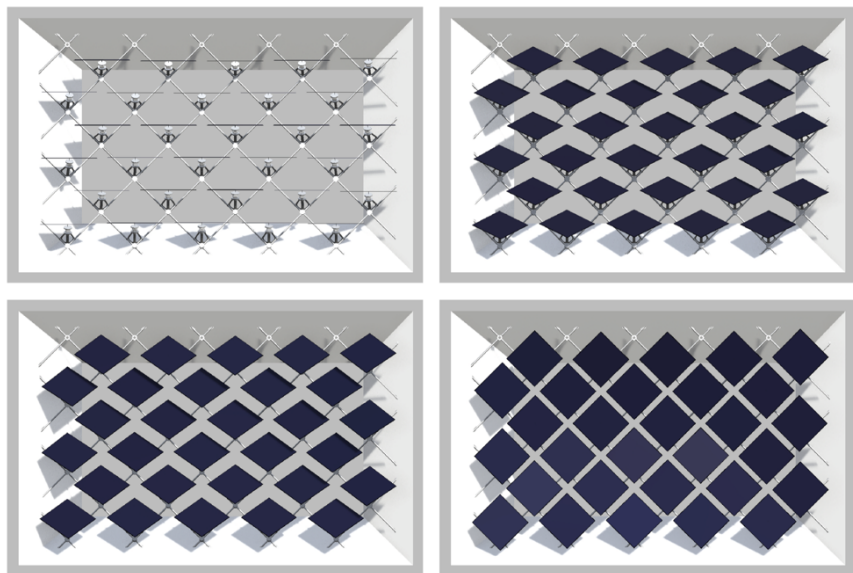


FIGURE 2.4: The Adaptive Solar Facade existing in varying states

ments to the mesh can be conducted to improve the architectural image. Each manual adjustment is directly computed by the second order FEA module, providing real time feedback about the stability of the adjusted structure. Figure 2.5 shows an example of this output with a list of simulation parameters. A load of 420N was applied on each panel node, which is equivalent to a category one hurricane on the Saffir-Simpson scale. The results are visualised in the form of coloured meshes which detail the utilisation factor in relation to the von Mises stress. A scaled down 2.2m x 1.5m prototype was constructed to validate the structural model.

2.2.2 Energy Evaluation

The evaluation of the energetic performance of the ASF can be found in [8], and will be briefly reviewed here for completion. This part of the PDE consists of five stages:

- 1. Solar Radiation Model:** The radiation on the PV panels and window behind the ASF is calculated for a single configuration of the ASF

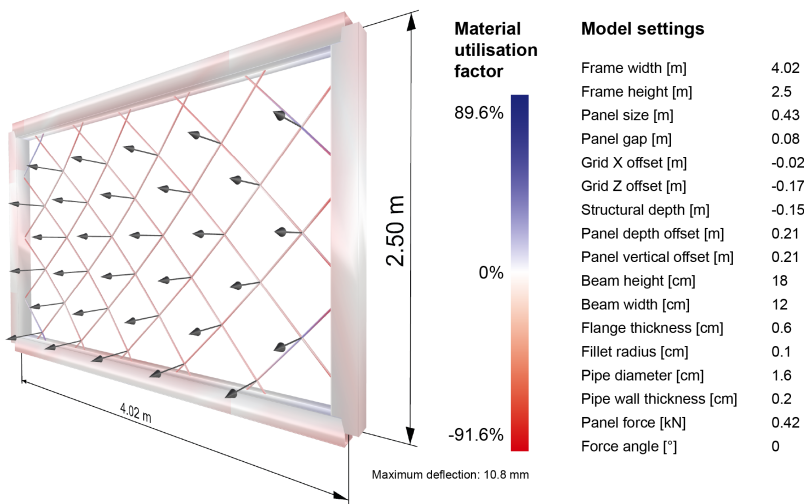


FIGURE 2.5: An example output from the Karamba structural simulation. The black arrows detail the loading direction, and the colour details the utilisation factor in relation to the von Mises stress. The table on the right details the input parameters to the simulation.

using the Grasshopper - LadyBug plugin for a single time step [23]. An example of the simulation result is shown in Figure 2.6.

2. **PV Electricity Production:** The radiation result is coupled to an electrical circuit simulation of monolithically interconnected, thin-film CIGS PV modules. This model takes into account the effects of module self-shading and temperature dependence [24].
3. **Building Energy Model:** The radiation calculated on the window surface is fed to a 5R1C single zone resistance-capacitance building model based on the ISO 13790 standard [25]. This calculates the heating or cooling demand of the building for the particular time step.
4. **Daylighting Model:** A linear daylighting model based on the total flux methodology is used to determine the luminosity in the room [26].
5. **Optimisation:** The simulation is conducted for all possible panel angle combinations based on the inputs to the parametric environment. The angle combination with the lowest net energy consumption is chosen for each time step. By summing all the time steps, the annual energetic performance of the ASF can be evaluated.

The source code for this methodology, with installation instructions can be downloaded from github [27, 28].

2.2.3 *Integration of classical design methods*

A purely parametric approach is very useful in investigating design possibilities, but once the concept needs to be put in practice, the parametric design environment needs to be complemented with physical prototypes, testing and classical design methods like simple 3D modelling and electronics design. As there is a trade-off between the flexibility of a parameterised environment and the time required for its development, it is important to wisely choose what to parameterise and what to design with classical methods. Parametrising the entire design process of complex systems such as an ASF can result in instabilities and lead to an increase in design time. For this reason, it is important to include certain constants amongst the parametric variables. Constants include the design of the electronics, connection details, and the actuator design [29, 30].

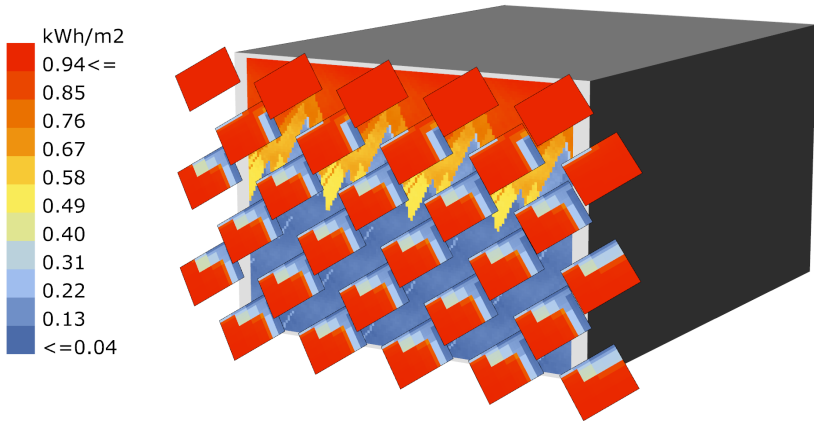


FIGURE 2.6: A simulation result showing the radiation on the solar panels and the window element on the 16 June 2013 between 12:00-13:00 in Zurich.

2.3 CASE STUDY

This section details some of the outcomes of the aforementioned design environment in relation to the case study at the HiLo building. In particular we will evaluate the optimal PV panel layout, the structure, details of the module design, and fabrication.

2.3.1 Optimum PV Panel Layout

The design of the PV panel layout is an example where all four stakeholders had inputs to the design. From an energetic perspective, a dense layout would have a larger overall PV surface area for electricity generation. However if the panels are too close together, there would be high module self shading which would lower the overall performance of the panels, as seen in Figure 2.7 [24]. Furthermore, there would be less natural lighting in the room, resulting in an increase of the building's overall energy consumption. From an architectural perspective, a sparse PV layout is preferred as it increases the transparency of the facade from the inside. This also lowers the

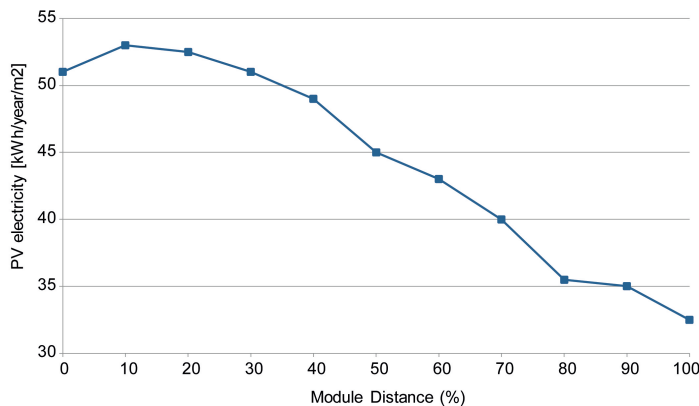


FIGURE 2.7: Effect of annual PV production with respect to module spacing per square meter of facade area [24]

overall cost, as less PV panels are required. Structurally, however, a sparse PV layout results in longer pipe elements between the junctions which lowers the overall strength, due to increased buckling length. Ultimately, a PV panel spacing of 510mm with a module size of 420mm was chosen as a trade-off between the above mentioned requirements.

2.3.2 Structure

With a frame size of 2.5×4.02 m, a PV panel spacing of 510 mm and a structural depth of the vault of 150 mm, the shape of the rod-net vault, the profiles of the pipes, and the size of the supporting frame was calculated. With a wind load of $0.92\text{KN} / \text{m}^2$, and a safety factor of 1.8, the finite element analysis concluded that the stainless steel pipe and the rectangular steel frame have a minimum dimensions of 16x2mm and 180x120x6mm respectively.

The relatively large frame is the result of a snap-through buckling failure criterion and relatively weak support conditions at the corners. As the vault is loaded, the large lateral forces on the frame result in deflections, which in turn reduce the depth of the vaulted structure. The reduced depth of the vault further increases the lateral loading, thus leading to a global snap-through buckling failure. The frame must therefore be large enough to withstand the maximum load criterion with minimal deflection. This

solution is characteristic to the conditions present on the HiLo building, where the ASF will be mounted with an offset of 80 cm from the building's support structure. In principle, the edge point of the pipe structure could be mounted directly to the support structure of the building, thus reducing the need for a frame. Figure 2.8a depicts how the utilisation of the pipe elements decreases with increasing frame strength, up to the point where all edge points are supported individually.

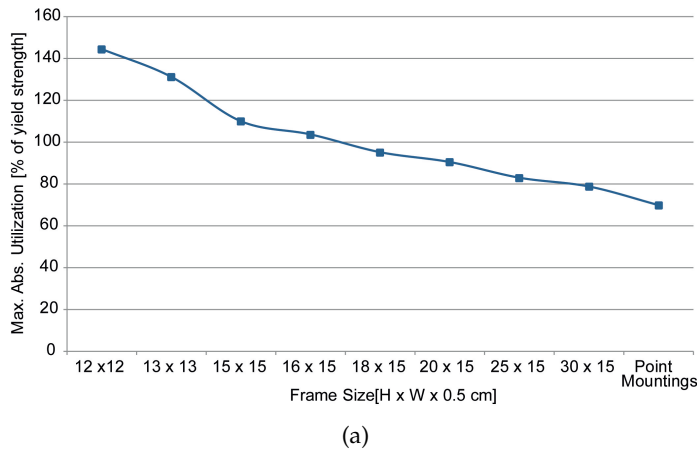
The 150 mm depth of the vaulted structure is sufficient to handle the wind loads with relatively thin pipes and minimal variation in the panel orientation. Ultimately, the choice of the structural depth is a trade-off between stability, self-shading, and aesthetics. A deeper structure offers more load bearing capacity requiring thinner pipes, however the self-shading of the panels increase. On the other hand, a shallow structure is less resilient to wind loads, leading to thicker pipes. The effect of the depth on the structural stability is depicted in Figure 2.8b. The image shows how the maximum utilisation of the pipes decreases with increasing structural depth, with a very steep decrease in the range of 12-15 cm.

The construction details contribute significantly to the overall stability of the structure and to the match between the real behaviour and the FEA simulation. For this reason, we designed the pipe and frame connections to provide a completely stiff connection under the assumed wind loads. To form the vaulted shape, each pipe element is bent close to its edges and kept straight in between those points to improve their stability to localised buckling.

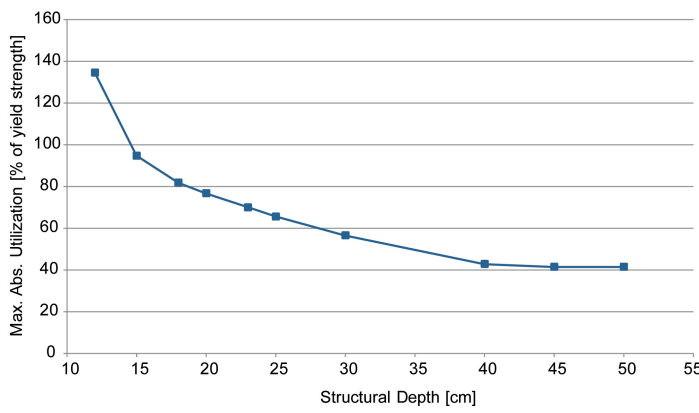
2.3.3 Structural Validation

A scaled down, 2.2m x 1.5m, prototype designed through the PDE was constructed for testing purposes. Weights were added to each of the seven junction nodes in 5kg increments until the structure collapsed as seen in Figure 2.9. Each junction node was also fitted with a deflection gauge.

The results of this analysis are summarised in Table 2.1. The simulated model underestimates the overall strength by 12% which is sufficient to validate our model. The deflection results, however, have a larger diversion. This diversion can be attributed to a weak construction joint at one of the edge nodes. The average deflection of the structure is 10.5mm which is close to the simulated model. Besides confirming the accuracy of the simulation, this test also confirmed the predicted snap-through buckling failure. Additionally, as seen in Figure 2.9d, the junction nodes, and frame



(a)



(b)

FIGURE 2.8: Utilisation factor, represented as a percentage of the maximum yield strength. Failure occurs with utilisation factors greater than 100%. The utilisation factor decreases with increasing frame size cross section, and with greater vaulted depth.

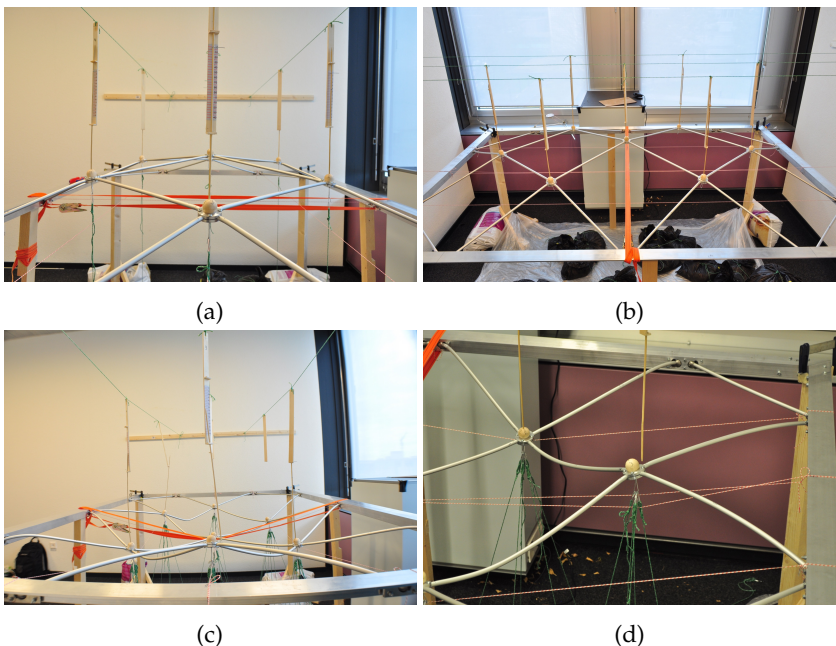


FIGURE 2.9: Prototype constructed for model validation. a,b details the experimental set up. c,d detail the snap-through buckling of the structure

connections were capable of resisting local torsion and maintained their position. The failure was localised at the pipes as predicted in Section 2.3.2.

2.3.4 Module Design

The kinetic PV module was then designed to fit within the requirements of the optimised layout and structure. The PV panels must be able to fully open, and fully close without making contact with the rod-net structure or other PV modules as shown in Figure 2.10. The PV panel is actuated using a soft pneumatic actuator [29]. The actuator is made from neoprene rubber and contains three air chambers. By pumping one or more of these chambers with compressed air, the actuator will deform, thus moving the panel with a 90° range in two degrees of freedom. The cantilevered bracket connects this actuator to the rod-net structure and holds it at a distance that prevents collision with other PV panels or the structure. A decentralised control box, located behind the junction element, contains three pneumatic

	Physical Model	Simulated Model	Deviation
Max Point Loading	250N	220N	-12%
Max Deflection	14.5mm	10.3mm	-29%

TABLE 2.1: Comparison of the physical and simulated model for the scaled down prototype

valves and an electronic board addresses the valves over a common data bus. This controls the flow of air to the chambers inside the actuator. An exploded view of the module is shown in Figure 2.11.

2.3.5 *Fabrication*

Once a design has been configured using the PDE, manufacturing plans can be automatically generated. This enables the plans to be immediately sent to manufacturers, without a significant time investment. This is especially important for components such as the steel pipes where each pipe has a unique length and bend angle. As an example, Figure 2.12 details four of the 92 pipe bending plans. Besides the plan, the PDE also generates a set of meta data that can be directly fed into a CNC pipe bending machine, thus simplifying the transition from design to production.

An ASF for the HiLo building was fabricated for testing purposes. The overall system took two people 11 days to construct, and was mounted onto a temporary concrete wall in one day, as seen in Figure 2.13. The design generated by the performative design environment was flawless. The ASF is currently undergoing tests to measure the electricity generation and adaptive control strategy. When the HiLo building is complete, it will be dismounted from its temporary location, and remounted in front of the south facing bedroom window of the HiLo.

2.4 DISCUSSION AND CONCLUSION

This paper presents a practical PDE for the design and fabrication of kinetic architectural elements. The PDE is capable of combining the multiple fields of structural engineering, energy engineering, control engineering, industrial design and architecture into one uniform environment, allowing the designers to handle the complexities of a multidisciplinary project.

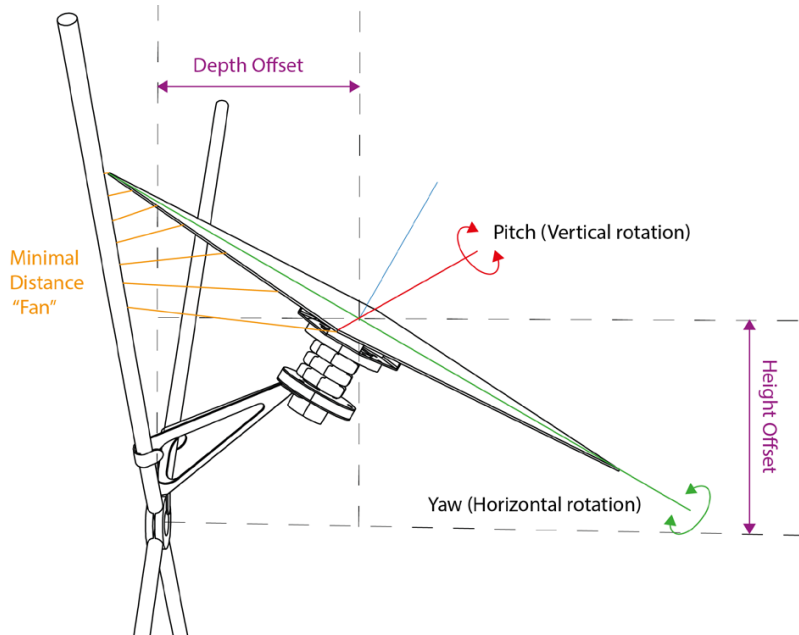


FIGURE 2.10: Constraints of panel motion relative to the structure

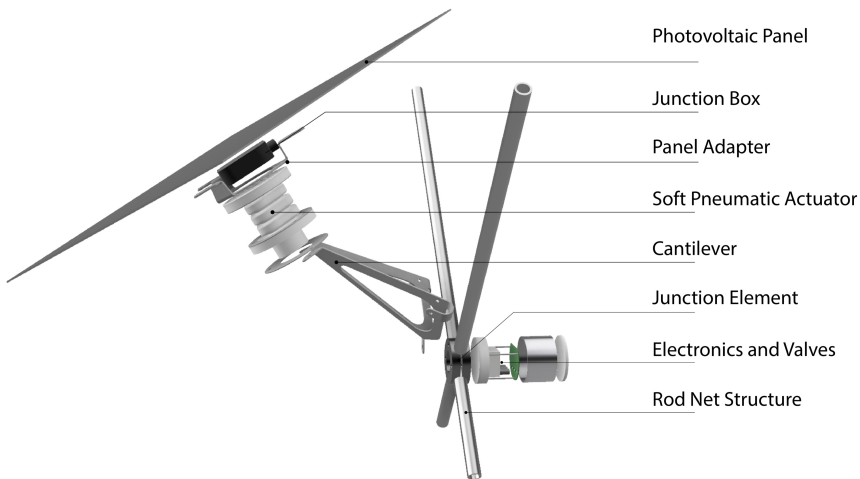


FIGURE 2.11: Exploded View of the final ASF Module

The major advantage of this environment is the considerable decrease in time between design iterations. Traditionally each of the respective stakeholders in the project would work on their individual design, and then exchange information in a meeting. With the PDE, the meeting is transformed from an information exchange session, to a design session where all stakeholders can collaboratively influence the design and immediately see the necessary results. What would normally take a month, was condensed to just a few hours. The design environment also develops with the project allowing for new parametric inputs, or new outputs to be created. This can be easily done with collaborative software management tools such as git.

One disadvantage is the overhead required to manage a PDE. Like a BIM manager, a PDE manager is required and must have a careful overview of the software. As the software ultimately determines the final form of the design, any errors in the software can be detrimental to the final design. It was therefore necessary for all stakeholders to conduct a final independent analysis prior to the submission of the final design.

It is also important to determine what aspects of the design should be contained within the PDE and what should be designed with classical methods. Essentially, all aspects where there could be conflicts between

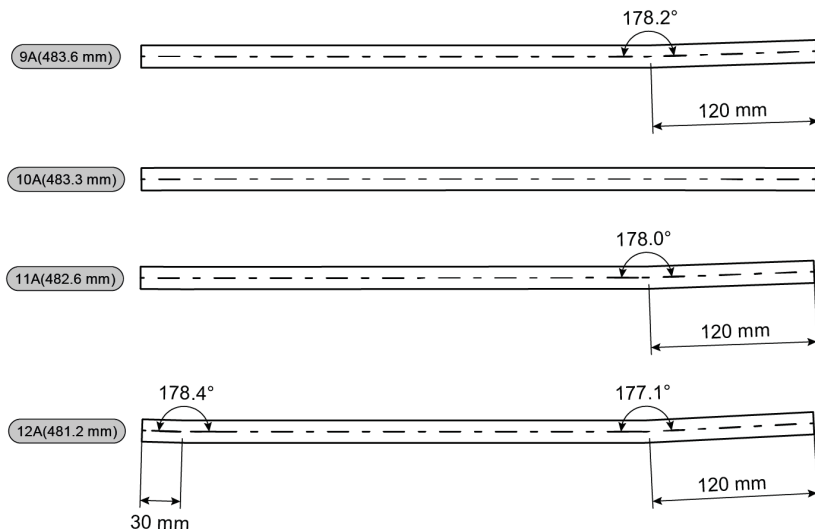


FIGURE 2.12: Automatically generated drawings for pipe bending. Here we show four of the 92 pipe drawings

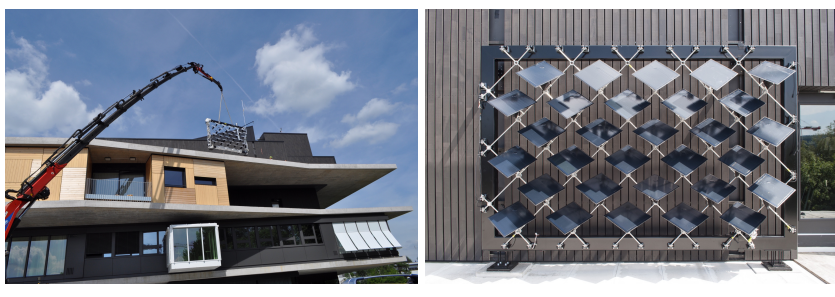


FIGURE 2.13: Mounting of a prefabricated ASF to the test site.

the stakeholders were included in the PDE, whereas many of the design details, such as the mounting brackets to the building, can still be designed independently and imported into the PDE as a static object. Over time, some static objects, such as the cantilevered bracket of the PV module became parametrised.

Ultimately, this paper presents a further step in the field of performative design by showing how a system as complex as a kinetic photovoltaic envelope, can be developed, prototyped and finally fabricated by a small team of four designers. The methodology can be utilised for any building component where multiple technological branches are required.

3

OPTIMISING BUILDING NET ENERGY DEMAND WITH DYNAMIC BIPV SHADING

The utilisation of a dynamic photovoltaic system for adaptive shading can improve building energy performance by controlling solar heat gains and natural lighting, while simultaneously generating electricity on site. This paper firstly presents an integrated simulation framework to couple photovoltaic electricity generation to building energy savings through adaptive shading. A high-resolution radiance and photovoltaic model calculates the photovoltaic electricity yield while taking into account partial shading between modules. The remaining solar irradiation that penetrates the window is used in a resistance-capacitance building thermal model. A simulation of all possible dynamic configurations is conducted for each hourly time step, of which the most energy efficient configuration is chosen. We then utilise this framework to determine the optimal orientation of the photovoltaic panels to maximise the electricity generation while minimising the building's heating, lighting and cooling demand. An existing adaptive photovoltaic facade was used as a case study for evaluation. Our results report a 20% - 80% net energy saving compared to an equivalent static photovoltaic shading system depending on the efficiency of the heating and cooling system. In some cases the Adaptive Solar Facade can almost compensate for the entire energy demand of the office space behind it. The control of photovoltaic production on the facade, simultaneously with the building energy demand, opens up new methods of building management as the facade can control both the production and consumption of electricity.

3.1 INTRODUCTION

Buildings are a critical element in our modern society and accommodate a variety of needs and functions. Unfortunately the energy consumed by buildings accounts for 32% of global final energy consumption and 19% of energy-related greenhouse gas emissions [3]. The existing building stock, therefore, offers a great potential for CO₂ mitigation of up to 50% - 90% using existing technologies [3]. Of these proposed technologies, building integrated photovoltaics (BIPV) have been recognised as a viable path to supply the energy needs of a building [31, 32].

Developments in efficiency and costs of thin-film BIPV technologies have brought new design possibilities [33–36]. Their lightweight and flexible nature allows for easier and more aesthetically pleasing integration into the building envelope. Furthermore, from a life-cycle perspective, there are attractive returns on embodied energy [37, 38]. One such example is the application of thin film PV on glazed surfaces to create a semi transparent BIPV system [39–41]. Such systems not only generate electricity, but also influence the thermo-optic properties of a building, which in Los Angeles can reduce the HVAC energy demand by 30% [42]. However, when used in colder climates, the reduction of solar heat gains results in a net HVAC loss [42].

Dynamic building envelopes can mitigate this loss by actively controlling direct and indirect radiation into the building, while still responding to the occupant's desires [6]. As seen in Figure 3.1 this mediation of solar radiation has the potential of improving daylight distribution, while simultaneously reducing heating and cooling demands [7]. Using thin film solar panels as our shading element also allows for the simultaneous production of photovoltaic electricity.

Previous research in this field can be divided into two categories: the integration of building energy performance simulation with shading, and the effects of BIPV on building energy performance.

With respect to the first category, the effects of external shading on building energy performance have been widely studied [43]. Palmero-Marrero et al. analyses the effects of external louvres using TRNSYS [44]. The paper shows that significant energy savings for space cooling is possible in hot climates, however in cities like London, the increase in the heating demand results in a net energetic loss. Nielsen et al. quantified the perfor-

mance of dynamic solar shading systems using both building thermal and daylight simulations with a case study in Denmark [45]. The results show that a dynamic shading system is the best design alternative as it has an improvement in daylighting performance over fixed shading systems.

Previous BIPV research analyses electricity production and building energy demand for static BIPV shading systems. Freitas et al. analyses different configurations of BIPV systems and shows that a tilted louvre configuration generates 20% - 40% more electricity than a flat vertical layout [46]. Sun et al. analyses a static tilted photovoltaic system mounted over windows and reports a 51.6% reduction in cooling demand [47]. Mandalaki et al. expands this analysis to 13 different types of shading devices with integrated PV [48]. Hu et al. combines PV production with building energy performance in an analysis of Trombe wall systems and finds that a Trombe wall with PV venetian blinds has a 45% energy saving when compared to classic PV Trombe wall systems [49]. Optimising the panel angles for PV production however are not always advantageous. Chatzipanagi et al. demonstrated that an inclination of 30° of integrated crystalline modules results in very high operating temperatures, thus penalising the system [50]. It is therefore important to also include thermal effects in BIPV analysis.

This paper expands on this previous research in two parts. Firstly, by combining the two aforementioned categories to evaluate a dynamic photovoltaic shading system and its interaction with the building energy demand. Secondly, by proposing a novel adaptive control strategy where the results of the simulation are used to determine the orientation of the PV panels. We have previously modelled the energy performance of dynamic BIPV shading systems [51]. The methodology was sufficient to attain an understanding of how such a system functions, however it used simplifications that ignored time-dependent characteristics of the building, such as thermal capacitance.

The contribution of this paper is a simulation framework that overcomes these simplifications, in order to evaluate the energetic performance of adaptive photovoltaic envelopes with respect to PV electricity production and building energy demand. We apply the framework in this paper in the context of the Adaptive Solar Facade (ASF) project, shown in Figure 3.2 [7]. The ASF is a lightweight PV shading system composed of dynamically actuated copper indium gallium selenide (CIGS) panels. CIGS panels

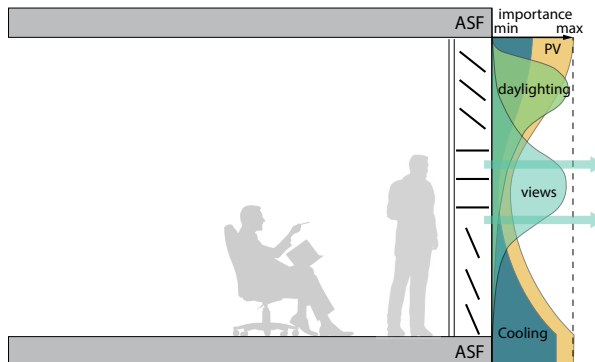


FIGURE 3.1: The facade acting as a mediator between the interior and exterior environment, while fulfilling various functions [7]

from Flisom were chosen due to their light-weight nature, high efficiency, and monolithic interconnection, however in principle any light-weight PV material can be used [52]. Each panel can independently rotate in two degrees of freedom, through the use of a soft pneumatic actuator [30]. This freedom enables local variations of the facade when reacting to internal and external factors. For more information on the technology, please refer to the publication by Nagy et al. [7].

The remainder of the paper is organised as follows. The next section describes the simulation methodology including the case study used in the analysis. In Section 3.3 we present the results of the case study which describes the adaptive response of the ASF to variations in the external and internal environment. Finally, Section 3.5 concludes the paper.

3.2 METHODOLOGY

The proposed framework is shown schematically in Figure 3.3. In brief, it consists of five stages. First, the radiation on the PV panels and office window is calculated for a single configuration of the ASF. The radiation results on the PV panels are then used to calculate the electricity generation. The radiation results on the window are imported into a building thermal model, and a separate lighting model. Finally, an exhaustive search of all possible configurations is performed to determine the optimal config-

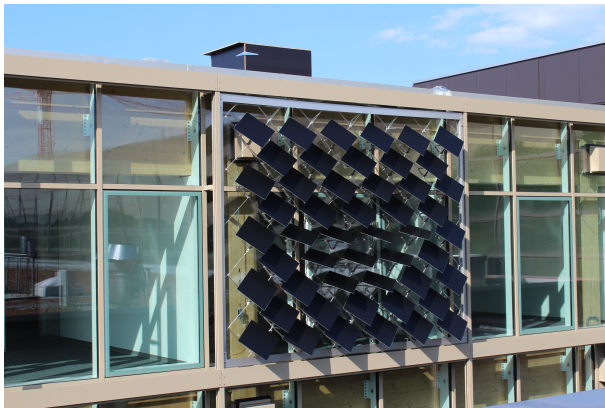


FIGURE 3.2: An example of an ASF constructed at the House of Natural Resources [7]

uration for maximum energetic performance. The framework along with installation guides are publicly available for download [27, 28]. The following subsections detail these five stages.

3.2.1 *Radiation Analysis*

A solar radiation simulation is run within the Rhino/Grasshopper environment [20] with the Ladybug plugin [23], that uses Radiance [53] to determine the incident insolation on the solar facade. The solar radiation analysis implemented in Ladybug is based on the cumulative sky approach [54] using the Perez All-Weather sky model and weather files with hourly resolution [55]. In this analysis, the sky is divided using the Tregenza scheme [56]. The approach enables us to calculate solar irradiance on the modules, and the glazed surface behind the facade. Self shading of the PV modules is inevitable as the gap between modules is only 100mm. The modules were therefore divided with a grid size of 25mm to include the effect of mutual shading as seen in Figure 3.4.

3.2.2 *PV Circuit Simulation*

The radiation results are coupled using Python to an electrical circuit simulation of monolithically interconnected, thin-film CIGS PV modules with

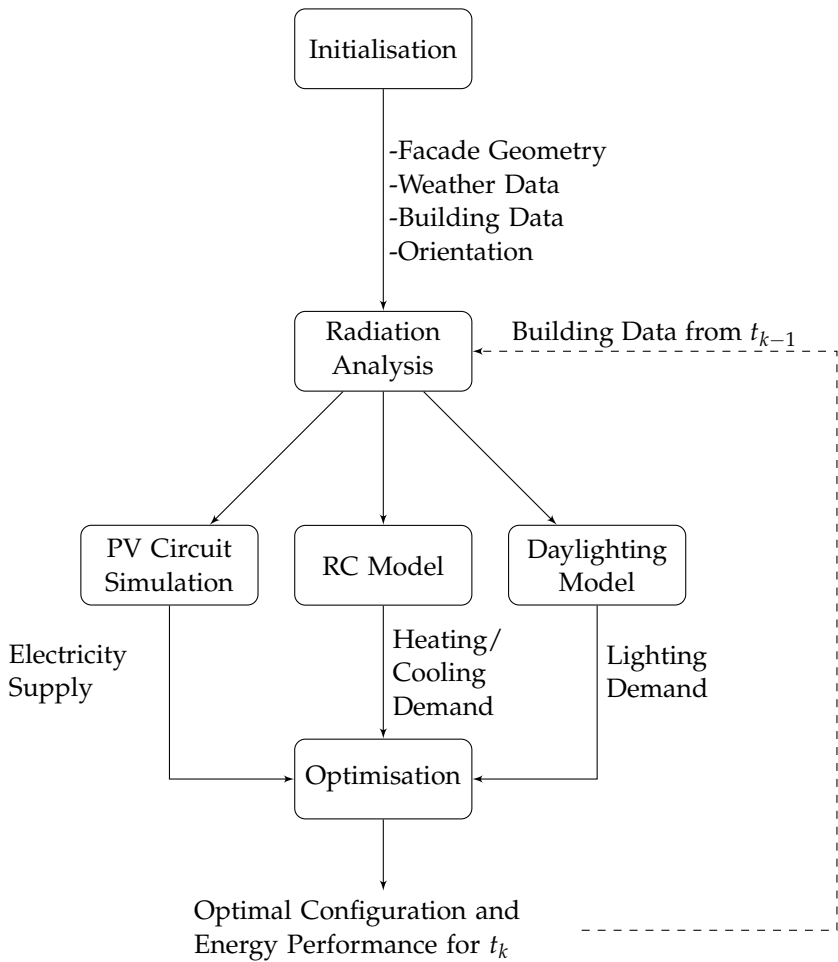


FIGURE 3.3: Simulation workflow

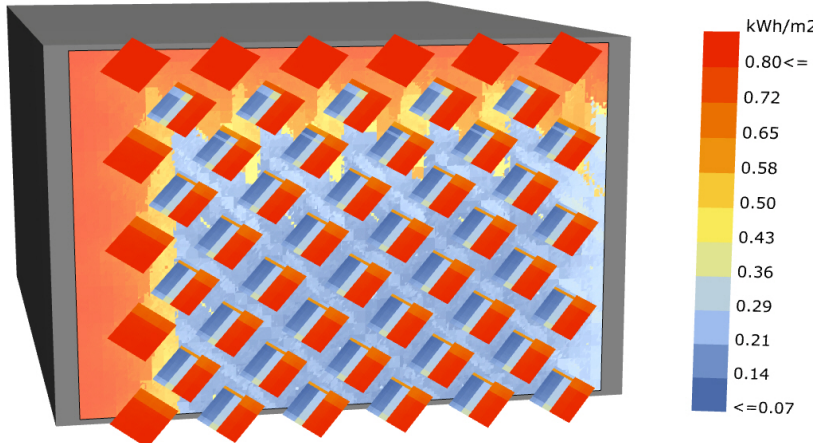


FIGURE 3.4: A simulation result showing module and window insolation from 11:00 - 12:00 on the 16 June for a Zurich weather file and a specific module orientation.

sub-cell level representation [21, 24]. This model uses the standard equivalent circuit model to calculate sub-cell current-voltage curves with a single diode, one series resistor, and one shunt resistor [57]. By doing so, the electrical losses through module self shading, as described in Section 3.2.1, can be taken into account. In addition to the irradiation dependency, the PV simulation includes temperature dependency. A linear relation between PV cell operating temperature and incident solar irradiance is assumed [58]. Infrared thermal imaging at different irradiance levels was used to infer the correlation factor. Electro-thermal effects and the influence of wind are neglected in the model. For more information, please refer to the publication by Hofer et al. [24].

3.2.3 RC Model for Building Energy Demand

This subsection describes the formulation of a physics-based model to simulate the thermal behaviour of the building using a resistor-capacitor (RC) model. This is based on an electrical analogy corresponding to the equivalent thermal physics [59–61]. The model, shown in Figure 3.5, consists of

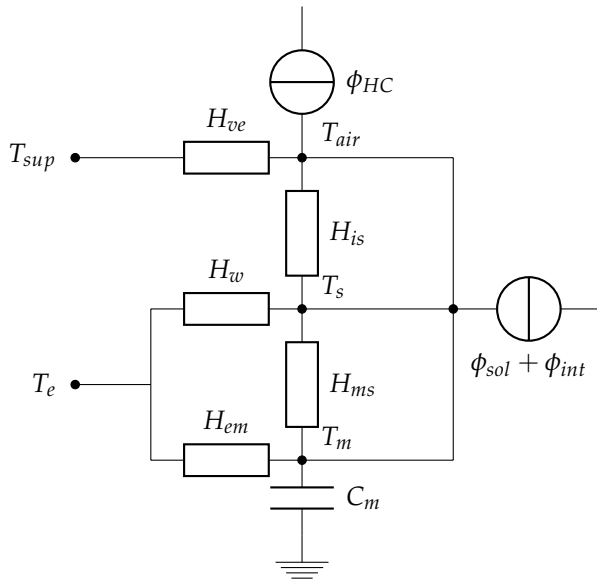


FIGURE 3.5: A 5R1C Model of the single zone office space

one internal thermal capacitance, and five thermal resistances. This is also known as a 5R1C model and is based on the ISO 13790 standard [25]. We will briefly review it here for completeness.

We assume that the only surface in contact with the external environment is the south facing glazed surface. All other surfaces of the room are in contact with other thermal zones of the building that we assume to hold the same room temperature. We therefore model them as adiabatic surfaces. Denoting by T_m , the temperature of the thermal mass in the room, the differential equation for the circuit in Figure 3.5 is given by

$$C_m \frac{dT_m}{dt} + T_m(H_{tr3} + H_{em}) = \phi_{mtot} \quad (3.1)$$

The value ϕ_{mtot} represents an equivalent thermal heat flux based on the solar heat gains, internal heat gains, external air temperature and the thermal conductances of the building elements. For this analysis we ignore any variations of air convection caused by the solar facade. For more information on this model, refer to the Appendix, or the source code on GitHub [28].

Equation 3.1 is discretised using the Crank-Nicolson method so it can be solved numerically as,

$$T_{m_{k+1}} = \frac{\phi_{mtot} + T_{m_k} \left(\frac{C_m}{\Delta t} - 0.5(H_{tr3} + H_{em}) \right)}{\frac{C_m}{\Delta t} + 0.5(H_{tr3} + H_{em})} \quad (3.2)$$

where the subscripts k and $k + 1$ refer to the timesteps of length Δt [62].

The heating or cooling demand for each time step is determined to ensure that the temperature $T_{m_{k+1}}$ is within the set thermal set points for occupant comfort. We assume that there is no restriction of the heating or cooling system. This means that the heating or cooling supply will always meet the calculated demand. The thermal demand is converted to electrical energy based on an average coefficient of performance (COP) of the heating or cooling system.

3.2.4 Lighting Model

Lighting control is based on the average luminance of the room. The luminance that passes through the solar facade, to the window, is calculated in the radiation analysis in Section 3.2.1. Using the total flux method [26], the total luminance per floor area is calculated by

$$\varphi_{flux} = \frac{E_w GMU}{A_{floor}} \quad (3.3)$$

where E_w is the incident illuminance on the window, G is the solar transmittance of the window, M is the maintenance factor which takes surface dust into account, and U is an empirical utilisation factor based on the room dimensions and ceiling profile. If the room luminosity is less than the set threshold for comfortable lighting, and there are occupants in the room, the lights are switched on to their maximum power. When compared against a more complex Radiance model with ambient bounces there was only a 5% divergence in results. The total flux method was therefore chosen due to its computational speed. This method however, is only applicable for small spaces. The evaluation of a hall, or an open plan working space would require a ray tracing analysis with multiple bounces. The electrical wiring and pneumatics of the ASF are encased within a reflective double curved stainless steel pipe structure that takes 6% of the projected area. We therefore assume that the influence of this structure is negligible.

3.2.5 *Exhaustive Search Optimisation*

At each time step we find the combination that minimises the net building energy demand, i.e. the difference of building energy demand for heating, cooling, lighting against BIPV electricity generation, using an exhaustive search of all possible configurations. Transient elements of the results, such as the temperature of the room, and thermal control settings are then stored for the next time step. It is also possible to run this optimisation to minimise individual objectives, such as heating alone.

3.2.6 *Case Study*

The ASF, shown in Figure 3.2, was constructed on the House of Natural Resources at the ETH Zurich [7]. We will use this system as a case study for the framework. The solar facade consists of 400mm CIGS square panels that can rotate in two degrees of freedom via a soft pneumatic actuator [30]. Each panel can be independently actuated with a continuous range of actuation. However, for simplicity, we group all the panels into one cluster that moves in unison with discrete angles. On the horizontal axis, the panels can move from 0° (closed) to 90° (open) position in steps of 15° . On the vertical axis, they can move from 45° to -45° in 15° steps. This results in 49 possible dynamic configurations of the facade system.

The studied building is a two person office which is 3.1m high, 4.9m wide, and 7m deep. Input data for the simulation is based on an energy plus weather file for the Zurich region [63]. The weather data is recorded at an hourly resolution, and therefore the simulation is also run at hourly timesteps. A full set of input parameters for this case study is summarised in Table 3.1.

3.3 RESULTS

In this section we show the results of the framework applied to the case study. Section 3.3.1 details the daily performance, this is then expanded in Section 3.3.2 for results spanning one year. Section 3.3.3 then compares this performance with a static shading system, and a facade with no shading. For each evaluation the thermal energy demands have been converted to an electrical energy input based on the coefficient of performance of the heating or cooling system.

Office Zone Settings	
Office Envelope	Internal Walls: Adiabatic Window: Double Glazed $U=1.1 \text{ W/m}^2\text{K}$ External Wall: $U=0.2 \text{ W/m}^2\text{K}$
Daylighting Variables	Glass Solar Transmittance: 0.68 Maintenance Factor: 0.9 Utilisation Factor: 0.7
Thermal Conductances	$H_{ve} = 39 \text{ W/K}$ $H_w = 14.9 \text{ W/K}$ $H_{em} = 0.34 \text{ W/K}$ $H_{is} = 491 \text{ W/K}$ $H_{ms} = 780 \text{ W/K}$
Thermal Set Points	Heating: 22°C Cooling: 26°C Set-Back: 4°C
Building System	Lighting Load: 11.8 W/m^2 Lighting Control Threshold: 300 lx COP Heating: 3 COP Cooling: 3
Occupancy	Office Schedule [64] Ventilation: 1.5 air changes per hour Infiltration: 0.5 air changes per hour Human Heat Emission: 120W per person
Location Assumptions	
Weather File	Zurich-Kloten, Switzerland 2013 [63]
Window Orientation	South

TABLE 3.1: Summary of simulation parameters

3.3.1 Daily Energetic and Control Profiles of the ASF

We run the optimisation for the net energy minimisation. The results, shown in Figure 3.6a detail the simulation run on a sunny day in winter. The dashed line details the optimum altitude angle from an open (90°), to a closed (0°) position, and the azimuth angles from a south-east facing (45°) to a south-west facing (-45°) direction. We can see that the azimuth angles start at an east facing position, roughly around 30° , and switches to a west facing position, around -30° in the afternoon. The building energy demand consists of heating (H) and lighting (L) loads in the morning and evening. We can see that between 10:00 to 15:00 the PV panels are capable of generating more electricity (PV) than the office requires.

Figure 3.6b compares this simulation with a sunny day in summer. The main energetic difference is the presence of a cooling (C) load in the afternoon. The panels still move in the azimuth directions from east to west, however the panels in the altitude direction sit at a higher angle to catch the higher sun position. The patterns in the summer and winter cases are representative of a solar tracking model, however, in both cases it appears to be limited between $\pm 30^\circ$. This is most likely due to high module self-shading at $\pm 45^\circ$, resulting in a large decrease in the PV module efficiency. In winter, the altitude angle is relatively stagnant at 15° . This angle is sufficient to maximise the PV electricity generation, while still allowing enough solar penetration into the room to keep the lighting and heating demands to a minimum.

In comparison, Figure 3.6c, details an optimisation on the same winter day, purely to minimise the heating load. In this case, the PV electricity generation, lighting demand, and cooling demand are not taken into account. There are two observable differences in the choice of angles. Firstly, the angles in the altitude position are mostly in the open (90°) position. Secondly, the azimuth angles follow an inverse solar tracking methodology, starting with west facing angles in the morning, and moving to east facing directions in the evening. Both effects maximise the solar penetration into the room and therefore minimise the heating demand (red line), at the expense of the PV electricity generation (gold line). A similar comparison was conducted for the summer case where a simulation was run purely to optimise the cooling load as seen in 3.6d. The optimum angles to minimise cooling are similar to the optimum angles to minimise net energy so there are only minor differences in the chosen angles.

It is also interesting to note that a sunny day in winter produces 3.0kWh of electricity, while a sunny day in summer produces only slightly more at 3.8kWh in the net energy optimisation case. This is due to the variation in the sun position. The low winter sun position combined with solar tracking means that the panels are often perpendicular to the direction of the solar radiation. In summer, on the other hand, there is a high sun position, resulting in module self-shading which decreases the efficiency of the PV panels. Over the full day, the PV electricity supply compensates for 62% of the energy demand on this sunny winters day, and 270% of the energy demand on a sunny summers day.

3.3.2 Optimum Annual Configurations

The optimal configurations of the ASF case study over a year can be visualised using heat-maps. Figure 3.7 and 3.8 detail the optimal angle in the altitude and azimuth angles respectively. To accelerate the radiation analysis, the weather data for each month is averaged to acquire data for a typical day of that month. Figure 3.7a-d detail optimisations of individual objectives. We can see how open configurations (light colours) are often chosen for the minimisation of the heating and lighting demands. Likewise, closed configurations (dark colours) are the preferred solutions to minimise the cooling demand during the summer months. Interestingly, this trend appears to inverse during the summer months at midday. The high sun position favours open positions to maximise shading thus minimising cooling in summer. Likewise closed positions with maximum tilt in the azimuth angle maximise solar penetration, and thus minimise heating. The grey coloured points indicate times where there is no sun and therefore the ASF has no influence on the results.

When the four optimisation cases are combined to achieve the configurations for total energy minimisation we get interesting results, as seen in Figure 3.7f and 3.8f. We see a clear tendency of the ASF to follow an optimal PV production pattern with the exception of the mid-winter evenings where heating and lighting are important. This means that it is energetically favourable to heat the room through solar radiation heat gains rather than converting the solar radiation into electricity which is then used for room heating. Configurations to reduce cooling demand are complimentary with the PV supply optimisation and therefore have a minor influence on the system control.

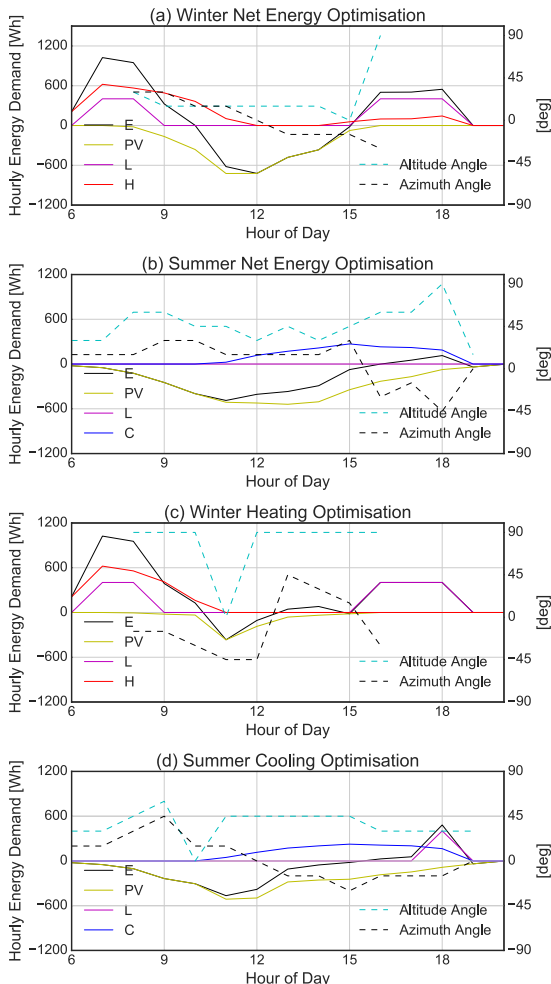


FIGURE 3.6: Net energy optimisation and adaptation of the ASF on a sunny day in winter (a) and summer (b). The solid lines detail the energy balance of heating (H), lighting (L), Cooling (C), PV electricity production (PV) and net energy (E) in Watt-hours. The dashed lines detail the panel position in the altitude angle from open (90°), to a closed (0°) position, and in the azimuth direction from a south-east facing (45°) to a south-west facing (-45°) direction. Only daylight hours are shown for the angle optimisation. In Figures (c) - (d) the optimisation is restricted to just the heating optimisation and cooling optimisation in winter and summer respectively.

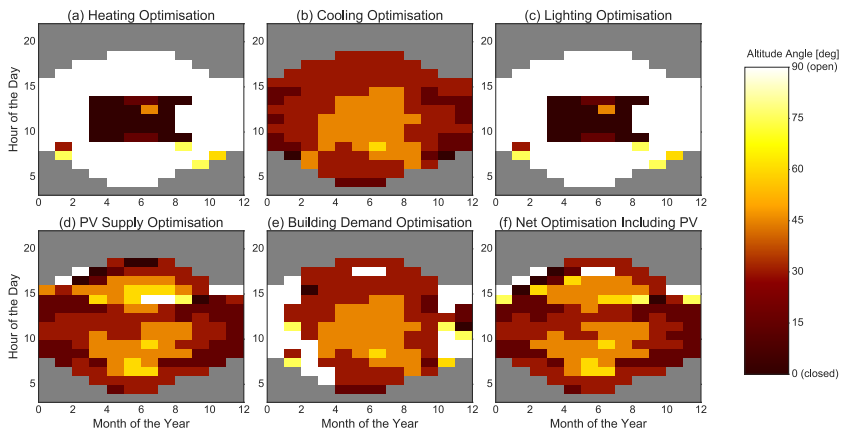


FIGURE 3.7: Carpet plots detailing the optimal altitude angles to minimise the heating demand(a), cooling demand (b), lighting demand (c), and maximise PV electricity production (d). (e) details the combinations for optimum building thermal management without PV production, (f) also includes the PV production. Small angles correspond to closed positions, whereas large angles represent open positions. The corresponding azimuth angles for each hour are shown in Figure 3.8.

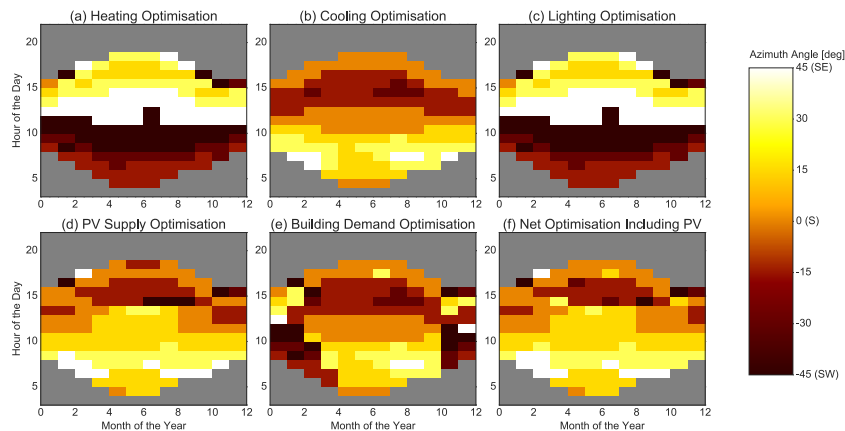


FIGURE 3.8: Carpet plots detailing the optimal azimuth angles to minimise the heating demand (a), cooling demand (b), lighting demand (c), and maximise PV electricity production (d). (e) details the combinations for optimum building thermal management without PV production, (f) also includes the PV production. Negative angles correspond to the panels facing west, whereas positive angles represent east-facing panels. The corresponding altitude angles for each hour are shown in Figure 3.7.

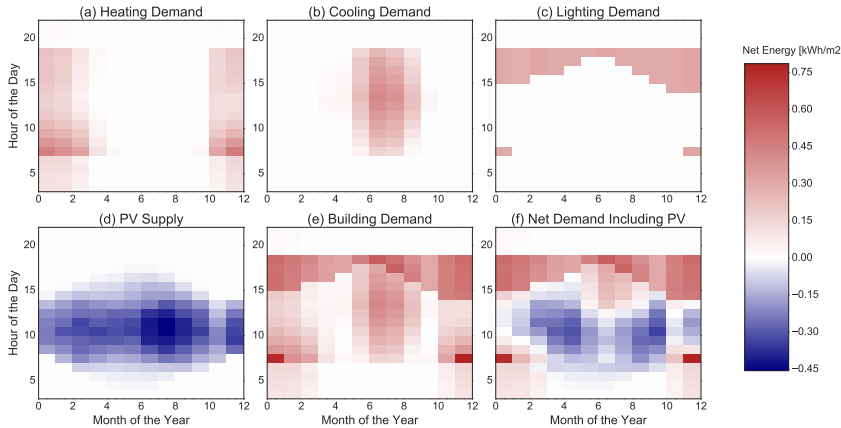


FIGURE 3.9: Carpet plots detailing the net energy consumption. Each square represents the total energy consumption for that specific hour of the entire month. Red colours detail net energy consumption, while blue colours detail net energy production.

Figure 3.9 shows the net electricity use. Red colours detail the electrical consumption intensity, and blue colours detail the PV electricity surplus. It is interesting to see in Figure 3.9f how the combination of electricity generation and adaptive shading can compensate for the energy consumption of the building during most sunlit hours. Overall the PV electricity compensates for 61% of the energy demand of the office behind the facade during the course of the year in the net energy optimisation case.

3.3.3 Comparison With Other Systems

Figure 3.10 shows the difference between a window with no shading system, a static shading system, and an adaptive shading system which minimised net energy demand, for various coefficients of performance of the heating and cooling system. The optimum orientation of the static shading system was calculated using the same simulation framework, and a panel inclination of 45° in the altitude direction is close to the energy optimal state.

Figure 3.10a details an example of an inefficient building system with resistive electrical heating and a low efficiency cooling heat pump. We can

$COP_{heating}$	$COP_{cooling}$	ASF vs No Shading (kWh/year)	ASF vs Static (kWh/year)
1	1	3750 (70%)	724 (31%)
1	3	1370 (62%)	670 (44%)
3	3	1560 (76%)	120 (20%)
6	6	1190 (97%)	145 (80%)

TABLE 3.2: Net electricity savings of the ASF to a building with no shading, and a static photovoltaic shading system in kWh/year.

see how having a simple static shading system can have a large reduction in the cooling demand with an increase in the heating demand. By including adaptability the same reduction in cooling is possible with a reduced increase in the heating demand. This effect becomes more pronounced in Figure 3.10b where a standard heat pump is added for cooling. Here the comparison between a static shading system and no shading is similar to the results obtained by Palmero-Marrero et al. where the reduction in the cooling demand is offset by the increase in heating demand [44]. An adaptive facade is able to negate this loss resulting in a 44% net energy saving compared to a building with a static facade. When an efficient heat pump heating system is also included, as detailed in Figure 3.10c, there is an increase in PV electricity supply by 19%, but a negligible change in the building energy demand. This is because the angles that maximise photovoltaic generation are preferred over angles that reduce the heating demand as there is a larger net energy saving. The same results apply to a highly efficient building case as detailed in Figure 3.10d. Interestingly in this case, the PV supply of the ASF can almost compensate for the entire energy demand of the office space behind it. The results are summarised in Table 3.2.

3.4 DISCUSSION

Our results show the advantages of an adaptive system to a static system with a 20% - 80% net energy saving potential. These results, however, are sensitive to the building system. Decreasing the efficiency of the heating, cooling or lighting systems will give higher preference for configurations optimised for building thermal management through adaptive shading over photovoltaic electricity generation. On the contrary, a highly efficient

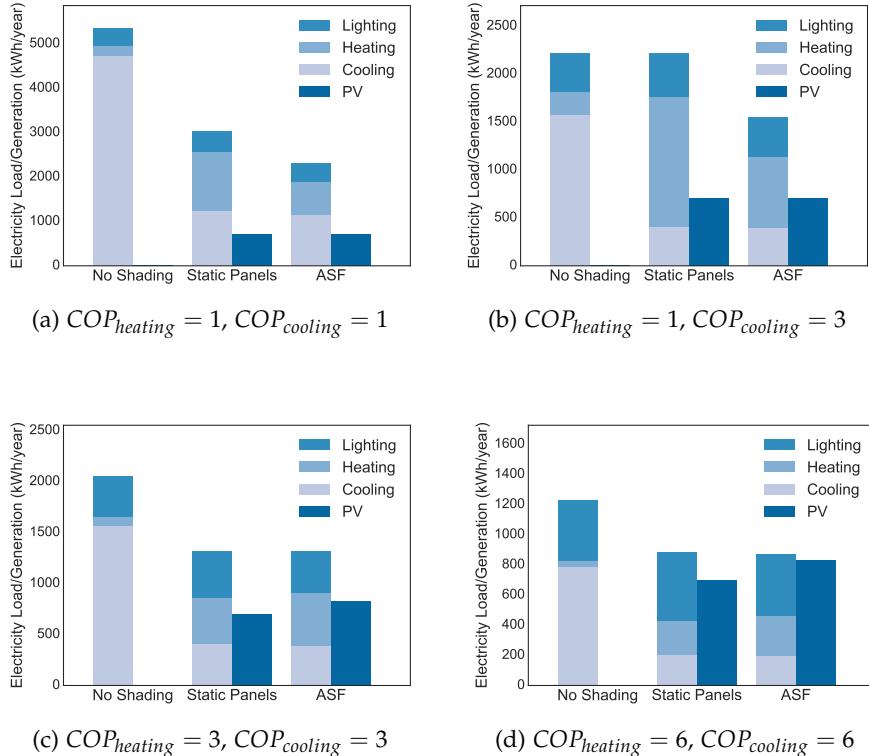


FIGURE 3.10: Breakdown of the operational electricity consumption with no shading, with static panels at 45° , and an ASF for different coefficients of performance of the heating and cooling system. (a) represents an inefficient heating and cooling system, (b) represents a standard cooling system with resistive heating, (c) represents a standard heat pump system for heating and cooling, and (d) represents a high efficiency heating and cooling system.

building system will show preference of the ASF to maximise PV electricity generation by following the sun. It is therefore important to run this framework for each individual building project to evaluate the cost-benefit ratio.

The results are also sensitive to the building location. Buildings in warmer climates, such as Miami have a large cooling demand and negligible heating demands. In such cases, from an energetic perspective, there would be a limited need for adaptivity. A static system comprising of semi transparent BIPV glass, or optimally tilted louvres would be a preferred solution. From the perspective of the user however, the ability to open or close the facade shading may be more favourable than having a fixed static system which blocks the views. The influence of occupant interaction has not been included in this study and will be evaluated through measurements of our constructed prototypes.

One bottleneck in this framework is the time required to compute the optimum set of angles. A computation of 49 configurations takes approximately 20 minutes, mainly due to the slow computational speed of the radiation analysis with shading. As a result, our angle resolution was limited to 15° . The radiation simulation could be accelerated by using parallel projection methods for the shading pattern calculation instead of having a discrete fine grid mesh on the PV modules. The overall computation speed could also be improved by using genetic algorithms over an exhaustive search. Through the use of these methods, a finer range of angles could be computed.

One limitation in the model is the daylighting model. The total flux method is chosen due to computational speed. However this does not apply for large open plan office spaces or halls. Furthermore, visual comfort issues such as glare can not be modelled with this method. Ray tracing methods, such as those utilised in the software package Radiance, can overcome this, but are too computationally intensive for this analysis. A custom radiation simulation using parallel projection methods for shading, as described earlier, may allow us to quickly evaluate the glare, and minimise its effect. The lighting is also currently modelled as a closed loop on-off system. By combining the system with variable lighting may lead to more efficient and interesting daylighting strategies.

One energetic loss in the system is due to self-shading between modules. When the model was run, purely to optimise photovoltaic electricity production, we see that the optimal angles do not follow a classic solar tracking model. Rather it follows a model similar to a two axis back tracking

system [65]. This is because a solar tracking model results in high module self-shading which reduces the overall efficiency of the PV panels. If the maximisation of PV electricity generation is the primary objective for the control of PV modules, a numerical approach based on a parametric 3D model as presented in this work, may be very effective to find solutions for complex tracking system geometries. The losses could be minimised in the design stage by increasing the spacing between PV modules.

Aside from the energy savings, the coupling of the PV electricity production with the building energy consumption brings new interesting building control strategies. For example, on a sunny winters day the facade can exist in an energy optimisation position to maximise the PV electricity yield while still enabling enough solar infiltration to keep the heating and lighting demands low. When the batteries are full, the facade can switch its optimisation strategy to positions that maximise the solar infiltration to the building, thus raising the thermal mass and reducing the evening heating demands.

3.5 CONCLUSION

In this paper, we have presented a framework to model the energy performance of an adaptive photovoltaic envelope. This is achieved through the use of Radiance for the radiation simulations, an electrical circuit simulation for the PV production taking into account effects of self-shading, and a resistor-capacitor model for the building simulation. An exhaustive search optimisation algorithm computes the most energy efficient system configuration for control by minimising the heating, cooling and lighting load, while simultaneously maximising the PV electricity generation. This framework can be applied to evaluate different PV system geometries, building systems, building typologies and climates.

Our evaluation of the Adaptive Solar Facade details the advantages of the adaptive system to a static system. The ASF is able to orientate itself to the most energy efficient position, thus finding the optimum balance between PV generation, and daylight control to minimise heating, cooling and lighting demands. When optimising for heating and lighting minimisation the ASF orients to open altitude positions at 90° to the vertical plane. When optimising for PV and cooling, the ASF selects closed position, between $15^\circ - 45^\circ$ to the vertical plane. When combining all objectives for net energy minimisation there is a tendency for the ASF to follow an optimal PV production pattern with the exception of winter evenings where it is

more favourable to utilise the solar heat gains for space heating and lighting. This result however, is only restricted to this case study. A less efficient heating system, for example, will result in the ASF existing in more open configurations to utilise the solar heat gains.

Our results report a 20% - 80% net energy saving compared to an equivalent static PV shading system depending on the efficiency of the building system. On a typical sunny winters day, the PV generation of the ASF can compensate for 62% of the energy demand, whereas on a sunny summers day, this rises to 270%. Over the course of the year, including cloudy days, the PV supply compensates for 61% of the annual energy demand. This can reach 95% in the case of a very efficient heating and cooling system with an average COP of six.

This work ultimately presents a framework for the planning and optimisation of sophisticated adaptive BIPV systems. Next stages of the research involve the utilisation of this model in our physical prototypes. The main difference in the physical model is the use of sensor data for the temperature and radiation values, as opposed to using a historical weather file. Furthermore, measuring the indoor temperature, PV electricity production, and lighting quality will create a closed loop feedback for model calibration and machine learning.

SENSITIVITY OF BUILDING PROPERTIES AND USE TYPES FOR THE APPLICATION OF ADAPTIVE PHOTOVOLTAIC SHADING SYSTEMS

An adaptive solar facade can improve building energy performance by controlling solar heat gains and natural lighting, while simultaneously generating electricity on site. The adaptive control of the solar facade is determined through an optimisation algorithm that minimises the net energy demand. In this paper, we first evaluate the sensitivity of the adaptive solar facade to the thermal performance of the building envelope for a south facing room in Zurich. We then evaluate the performance of an adaptive solar facade on 11 building use types spanning six construction periods. In addition, we compare the performance of an adaptive system against an equivalent static photovoltaic system, and a facade with no shading system. Our results show that the adaptive solar facade performs best in buildings that have a high cooling demand and low heating demand. This is because the optimum configurations for cooling minimisation generate the maximum photovoltaic electricity. As a result, we notice a higher energy saving potential in newer buildings with low envelope thermal transmittance (U-value or infiltration). However, in buildings with a very high cooling demand, and no heating demand, there is only a small improvement in performance compared to an equivalent static system. An adaptive solar facade is therefore an optimum solution when there are both heating demands, and cooling demands present. Modern offices, retail stores, food stores, and schools have this property and perform well with an adaptive solar facade compared to an equivalent static system, and a facade with no shading.

4.1 INTRODUCTION

The built environment is responsible for 19% of global greenhouse gas emissions [3]. Fortunately, the use of existing technologies such as building integrated photovoltaics (BIPV), thermal insulation, and efficient building systems can mitigate up to 50%-90% of this emission portfolio [3].

Thin film photovoltaics (PV) in particular have improved in terms of efficiency, cost, and light weight integration [33–36], which influenced the development of the adaptive solar facade (ASF) [7]. The adaptive solar facade consists of an array of independently actuated photovoltaic panels that can move in two axes at a range of 90°. An example of this technology was built at the House of Natural Resources at the ETH Zurich Campus as seen in Figure 4.1. Through the control of solar radiation, the ASF is capable of minimising the building energy consumption in terms of heating, cooling and lighting demands, while simultaneously generating electricity on site.

The optimum panel angles of the ASF are determined through a model control algorithm [66]. Simulations of building energy performance and photovoltaic electricity supply are performed for every possible combination of angles for each time step. Through an exhaustive search, the optimum combination is chosen. An ASF built on a building with an inefficient heating system will tend to exist in a more open position in winter so that the room can heat naturally through solar radiation. Likewise, a building with an efficient heating system will tend to optimise more for the generation of electricity on site. This sensitivity to the building typology leads to an energy saving variation of 20% - 80% compared to an equivalent static system [51, 66].

This paper utilises the models proposed by Jayathissa et al. [66] to extend the evaluation to a variety of building archetypes in Zurich. We will first evaluate the sensitivity of the ASF performance to the envelope resistance, and infiltration. We will then evaluate 11 building use types spanning six construction periods from the City Energy Analyst (CEA) for ArcGIS database [67]. By doing so, we can evaluate the optimum building properties and types for the application of an ASF.

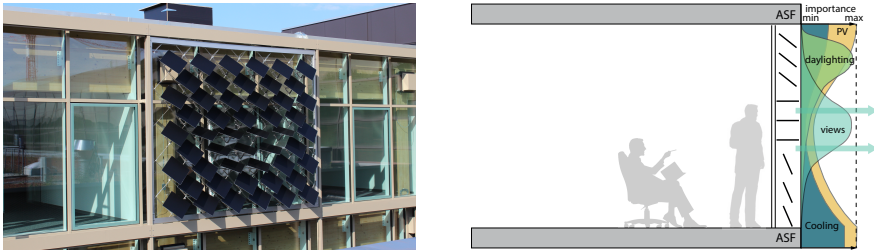


FIGURE 4.1: Left: An example of an ASF constructed at the House of Natural Resources. Right: a schematic describing how the facade can mediate solar radiation to optimise the internal environmental conditions [7]

The remainder of the paper is organised as follows. The next section describes the simulation methodology. In Section 4.3 we present the results of the case study which describes the sensitivity of the ASF to the building typology. Finally, Section 4.4 concludes the paper.

4.2 METHODOLOGY

A control methodology of adaptive photovoltaic shading systems to maximise PV electricity production while minimising the building energy consumption was proposed by Jayathissa et al. [66]. It will be briefly reviewed here for completeness.

- **Solar Radiation Model:** The radiation on the PV panels and window behind the ASF is calculated for a single configuration of the ASF using LadyBug/Radiance for a single time step of one hour [23, 53].
- **PV Electricity Production:** The radiation result is coupled to an electrical circuit simulation of monolithically interconnected, thin-film CIGS PV modules. This model takes into account the effects of module self-shading and temperature dependence [24].
- **Building Energy Model:** A 5R1C single zone resistance-capacitance building model based on the ISO 13790 standard computes the heating or cooling demand of the building for the particular timestep [25]. We assume that the only surface in contact with the external environment is the south facing glazed surface. All other surfaces are in contact with other thermal zones and modelled as adiabatic surfaces.

The climate in Zurich is defined as an oceanic climate (Cfb) by the Koeppen Index with an average July temperature of 18.4°C, and January temperature of 0.2°C [68].

- **Daylighting Model:** A linear daylighting model based on the total flux methodology is used to determine the luminosity in the room [26].
- **Optimisation:** The simulation is conducted for all possible panel angle combinations. The angle combination with the lowest net energy consumption is chosen for each timestep.

4.2.1 Sensitivity Analysis

Sensitivities in the framework can be modelled by adjusting variables in the resistor-capacitor model. Two envelope sensitivities will be analysed in this study

- **Envelope Thermal Transmittance:** The building envelope is characterised in the RC model as H_w which is the U-value of the envelope.
- **Infiltration:** The infiltration rate is modified as an air exchange conductance in the ISO RC model H_{ve} [25, 66].

This quasi-conductance is modelled as

$$H_{ve} = \frac{\rho c_a V_{room}}{3600} \left[ACH_{infl} + ACH_{vent}(1 - \eta_{vent}) \right] \quad (4.1)$$

where:

ρc_a is the heat capacity per air volume = 1200 J/(m³K);

η_{vent} is the efficiency of the ventilation heat recovery unit

ACH_{vent} is the air changes per hour for ventilation of the room volume V_{room}

ACH_{infl} is the air changes per hour for the infiltration of the room volume V_{room} which is the variable in this sensitivity analysis

4.2.2 Analysis of Archetypes

Building envelope parameters are imported from the CEA Toolbox, an open source urban building simulation software. The archetype databases

are publicly available on the CEA GitHub page [64, 69]. From this data, the following variables are evaluated: envelope U-value, occupancy profile, human heat emissions, lighting control set point, lighting load, thermal set points, and building thermal capacitance.

One critical component not analysed in the evaluation is the window to wall ratio. This was kept constant to maintain a valid comparison.

4.3 RESULTS

4.3.1 *Sensitivity of the Building Envelope*

Figure 4.2a details the performance of the ASF constructed on a typical office building with respect to the envelope U-value. As expected the heating demand increases with increasing U-value. Interestingly, the photovoltaic electricity supply decreases. This is because the ASF always optimises for net energy minimisation. With increasing heating demands, the ASF will optimise for positions that direct solar radiation into the building to minimise the heating loads as opposed to generating the electricity on the panels. This same characteristic is apparent in 4.2b which compares the energy saving potential of the ASF compared to a glazed facade with no shading system. A building with low envelope U-value will have a large saving potential due to the reduction of cooling loads, and supply of photovoltaic electricity. As the envelope U-value increases, this saving potential begins to decrease.

Figure 4.2c compares the ASF to an equivalent static photovoltaic shading system with panels orientated in the most energetically favourable position. As the U-value increases the net energy saving increases. As mentioned earlier, the heating demand increases with increasing U-value. For high U-value envelopes, the ASF will adapt and open up the panels thus reducing the heating demands. The equivalent static system will remain in a semi closed position for the entire year, and will block the solar heat gains necessary in winter.

Figure 4.3 details the equivalent analysis with varying infiltration rates. Similar trends can be observed to those in Figure 4.2. Leakier buildings lead to high heat demands, which decreases the performance of the ASF compared to a glazed window with no shading, but increases the performance relative to a static shading system.

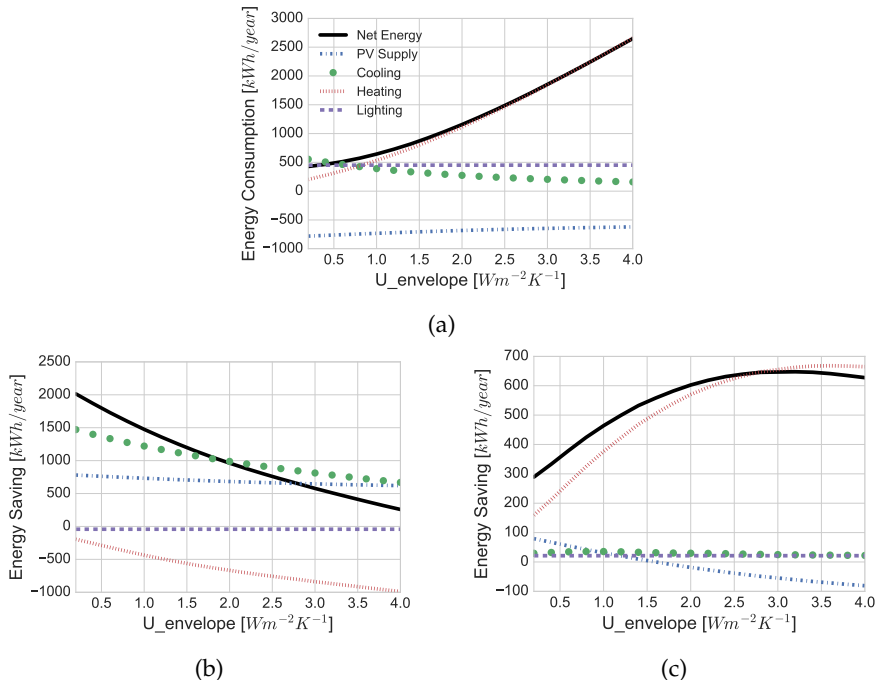


FIGURE 4.2: Influence of envelope thermal transmittance (U -value). a) Details the energetic performance of the ASF with respect to building envelope U -value. b) compares the energy saving potential of an ASF relative to a facade with no shading system. c) compares the energy saving potential of an ASF relative to an equivalent static PV system.

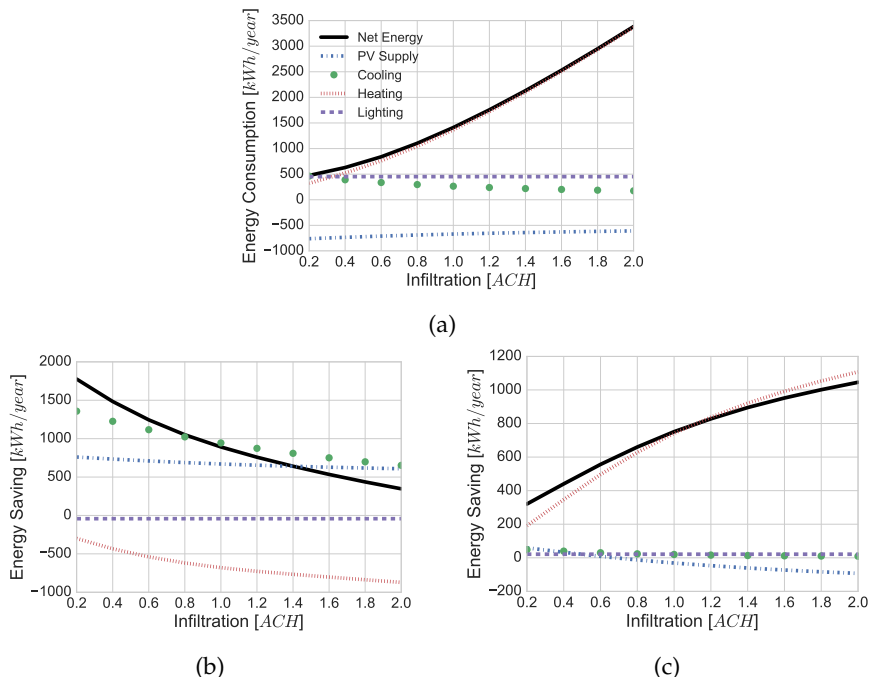


FIGURE 4.3: Influence of infiltration. a) Details the energetic performance of the ASF with respect to building infiltration. b) compares the energy saving potential of an ASF relative to a facade with no shading system. c) compares the energy saving potential of an ASF relative to an equivalent static PV system.

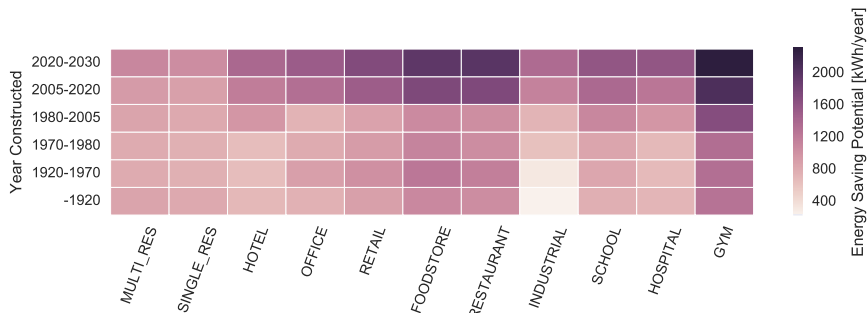


FIGURE 4.4: Annual results detailing the energy saving potential of the ASF vs a glazed window with no shading system

4.3.2 Archetype Evaluation of the ASF

Figure 4.4 compares the energy saving potential of 11 building use types with six different construction periods compared to a glazed facade with no shading system. Darker colours indicate larger energy saving potentials. One clear trend is the increasing saving potential in newer buildings over older buildings. This can be attributed to the lower envelope U-value in newer buildings, which as discussed in Section 4.3.1 will increase the energy saving potential. It is also interesting to note that the ASF performs best in gym use types. Gyms have a large cooling demand due to the high human heat emissions. Optimum configurations for cooling minimisation generates the maximum photovoltaic electricity supply.

However, an ASF is not necessarily the best design solution for buildings with a large cooling demand. Figure 4.5 compares the ASF performance against an equivalent static system. If we once again focus on the modern gym, we notice that there is only a small increase in the energy performance of an adaptive system over an optimally configured static system. When comparing both heat maps we see that an ASF performs best on in a modern office, retail store, food store, and school. These archetypes perform well due to two reasons. Firstly, they have an even balance of heating and cooling demands. Thus there is a need for adaptivity in the envelope to reduce these demands. Secondly, these archetypes are in use during the day. Residential buildings on the other hand are mostly occupied at night where the ASF has no influence on the building performance.

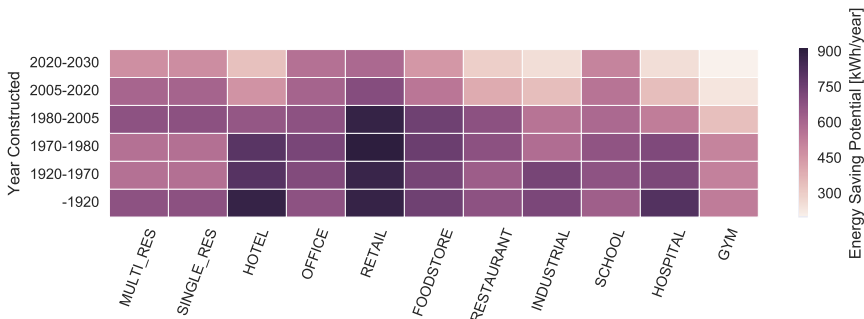


FIGURE 4.5: Annual results detailing the energy saving potential of the ASF vs a static photovoltaic shading system

4.4 DISCUSSION AND CONCLUSION

In this paper, we have evaluated the energetic performance of the adaptive solar facade (ASF) over 11 building archetypes spanning six construction periods. We notice that the ASF performs most efficiently in an environment dominated by cooling demands as the angles of photovoltaic panels to reduce the cooling demand also maximise the photovoltaic electricity supply. When compared to a plain glazed facade with no shading system, we observe large energy saving reductions in buildings that have high cooling demands and low heating demands. When compared to an equivalent static photovoltaic shading system, the inverse is true: larger energy saving potentials are present in buildings with low cooling demands and high heating demands. This is because the static system is not capable of opening its panels during times where heating is required, thus disadvantaging buildings with a large heat demand.

For shading system designers, there is an important balance between the building archetype and the type of shading system to be used. For buildings with poorly performing envelopes, maximising solar heat gains is important to reduce heating loads. A window without shading, or a system with manually controlled Venetian blinds may be the optimal solution. Modern buildings with good insulation and large heat gains have a high cooling demand. In these cases, the ASF performs very well and would be a recommended solution. However, when the cooling demands are very

high, such as in a modern gym, it would be more cost effective to install a simpler, static photovoltaic shading system at an optimum solar angle.

Further expansion of this research should be conducted to evaluate the impact of the building system. Increasing the efficiency of the heating, cooling, or lighting system will give higher preference for configurations optimised for photovoltaic electricity generation over building thermal management.

The analysis ultimately helped to clearly identify possible application cases of an adaptive solar facade with the highest benefit in terms of energy efficiency. The methodology proposed may also be useful for the identification of suitable application cases for other shading system types.

5

LIFE CYCLE ASSESSMENT OF DYNAMIC BUILDING INTEGRATED PHOTOVOLTAICS

We assess the environmental impact of a dynamic, adaptive, building integrated photovoltaic (BIPV) systems. Such systems combine the benefits of adaptive shading with facade integrated solar tracking, thus reducing the building energy demand, and simultaneously generating electricity on-site. The inventory for the life cycle assessment (LCA) was acquired using production data, and Energy Plus simulations to calculate the building energy demand. The impact assessment was conducted according to ISO 14040 and ISO 14044 standards using the Eco-invent database and openLCA as an analysis tool. The embodied environmental impact of the dynamic BIPV solution is higher than a static alternative due to the added control system, electronics, actuators, and additional supporting structure, resulting in higher life cycle impacts. However when accounting for the systems multi functionality aspect, i.e. savings through adaptive shading to the building's heating, cooling and lighting loads, the embodied environmental impact can be offset, making the ASF an interesting alternative for BIPV. We also conduct a sensitivity analysis to investigate modifications to the actuator type, control system, and location and find that none of the investigated parameters overturn the key findings. The analysis ultimately enables us to provide design recommendations for future dynamic BIPV installations.

5.1 INTRODUCTION

Buildings are at the heart of society and currently account for 32% of global final energy consumption and 19% of energy related greenhouse gas emissions [3]. Nevertheless the building sector has a 50-90% emission reduction potential using existing technologies, and widespread implementation could see energy use in buildings stabilise or even fall by 2050 [3]. Within this strategy, building integrated photovoltaics (BIPV) has the potential of providing a substantial segment of a building's energy needs [31]. Even the photovoltaic (PV) industry has identified BIPV as one of the four key factors for the future success of PV [32].

Recent developments regarding efficiency and costs of thin film BIPV technologies, in particular, CIGS, have brought new design possibilities [33-36]. Their lightweight nature and customisable shapes allow for easier and more aesthetically pleasing integration into the building envelope. In addition, less power is required to actuate them, thus facilitating the development of dynamic envelope elements due to their reduced weight [70].

Dynamic buildings envelopes have gained interest in recent years because they can save energy by controlling direct and indirect radiation into the building, while still responding to the desires of the user [6]. This mediation of solar insolation can offer a reduction in heating / cooling loads and an improvement of daylight distribution as seen in Figure 5.1 [70]. Interestingly the structure and mechanics required for dynamic envelopes couples seamlessly with the structure and mechanics required for facade integrated PV solar tracking. The use of light weight PV as an adaptive envelope material enables it to also benefit from on-site energy production. Furthermore, it provides a new way of aesthetically integrating PV panels onto buildings. The balance of electricity production and adaptive shading can in some cases offset the entire energy demand of an office space behind the envelope [71]. We have proposed one possible combination of these technologies as an Adaptive Solar Facade (ASF) [7]. An example of an ASF can be seen in Figure 5.2.

The design of an ASF comes at an added cost. The additional electronics, actuators, and supporting structure adds further embodied CO₂ to the product. It is therefore important to conduct a life cycle impact assessment (LCA) to analyse whether the life cycle environmental impacts are favorable, compared to a more classic system. It is also important to see

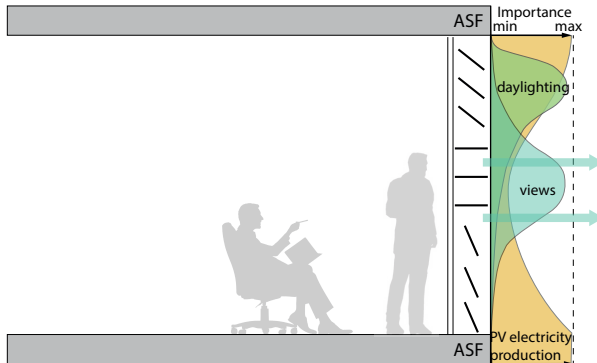


FIGURE 5.1: The facade acting as a mediator between the interior and exterior environment, while fulfilling various functions [7]

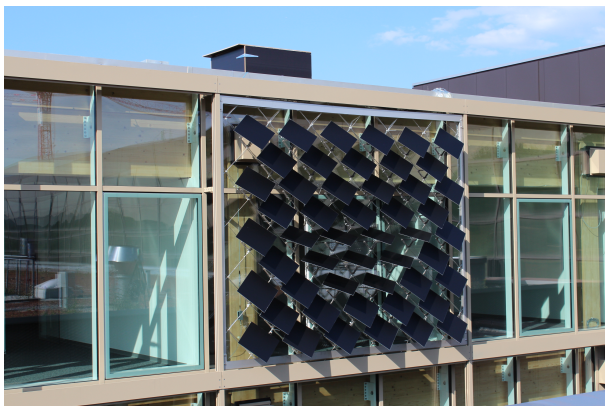


FIGURE 5.2: An example of an ASF constructed at the House of Natural Resources [7]

how variations in design can alter the green house gas (GHG) reduction potential of the technology. Aspects such as the chosen actuator, control system, and location of operation can have an impact on environmental performance.

The state of the art literature assesses existing photovoltaic technologies [72–74], and the balance of systems (BOS) which includes all other components of a photovoltaic system [75]. This has not however, been expanded to dynamic BIPV systems, and in particular, systems that combine the benefits of adaptive shading and electricity production.

In this paper, we investigate the environmental performance of an ASF and compare it to existing static photovoltaic systems. We also investigate 1) a system expansion including the heating ventilation and air conditioning (HVAC) savings through adaptive shading 2) design variations of the ASF, 3) the operational emissions of a building, with and without an ASF, and 4) the sensitivity of the LCA to its location and design.

The remainder of the paper is organized as follows. The following section introduces the ASF and the used LCA methodology. In Section 5.3, we present the results of the LCA analysis. Section 5.4 discusses the results and provides design guidelines. Section 5.5 concludes the paper.

5.2 METHODOLOGY

In this section, we detail the inventory, Energy Plus simulation methodology, important assumptions, and the LCA evaluation method. The assessment considers the environmental impacts of the production, operation, and disposal of an ASF. We assume a lifetime of 20 years based on the product warranty of the PV panels. The impact assessment is performed according to the ISO 14040 and ISO 14044, and is performed in four stages: (1) Goal and Scope Definition, (2) Inventory Analysis, (3) Impact Assessment, and (4) Interpretation [76].

1. GOAL AND SCOPE DEFINITION : This paper primarily assesses carbon emission reductions therefore the global warming potential (GWP) impact category is primarily assessed. The assessment also looks at six other major ReCiPe midpoint indicators: terrestrial acidification potential (TAP), freshwater eutrophication potential (FEP), human toxicity potential (HTP), metal depletion potential (MDP), and photochemical oxidant formation potential (POFP). These categories are

most relevant to the technology and most widely used in existing literature [77]. The functional unit is the electrical power production of the system in kWh.

The scope of the assessment, respectively the system boundary, is summarised in Figure 4. We analyse the manufacture, dynamic actuation, maintenance, and disposal of the solar facade. The scope comprises of a cradle-to-grave approach, where transport to and from site is taken into account. In order to account for the multi-functionality aspect of the ASF (i.e. electricity production and shading benefit), we carry out a sensitivity analysis and expand the system boundary including operational energy savings through adaptive shading. As the life cycle inventory (LCI) background database we use Ecoinvent v3.1 [78] with the cut-off system model ¹. That means impacts are allocated to the primary use of the product and it receives no credit for the provision of recycled material. Once a product is disposed or recycled, it leaves the system boundary and the recycled product comes “burden-free”.

2. INVENTORY ANALYSIS : The Ecoinvent v3.1 database is used as the main LCA database [78]. A detailed description of the inventory is found in Section 5.2.1 and 5.2.2.
3. IMPACT ASSESSMENT : The assessment is based on the IPCC 2007 methodology [79]. The GWP assessment is performed using the OpenLCA assessment tool [80]. In the assessment, we also compare the emission factor (EF) of an ASF with other PV systems. The emission factor is expressed as

$$EF = \frac{GWP}{G} \quad [\frac{kgCO_2-eq}{kWh}] \quad (5.1)$$

where (G) is the electricity production in (kWh).

4. INTERPRETATION : The results of the LCA analysis (not including shading effects) are compared with other facade integrated PV technologies. We then perform a system expansion to also include the effects of adaptive shading to the system. Finally a sensitivity analysis is conducted which is further described in Section 5.2.3.

¹ <http://www.ecoinvent.org/database/system-models-in-ecoinvent-3/cut-off-system-model/allocation-cut-off-by-classification.html> - Accessed: 8.2.2016

5.2.1 Embodied Life Cycle Inventory

The mechanical components of an ASF can be broken into four parts: a PV panel, actuator, cantilever, and a cable net supporting structure. The PV panel, actuator and cantilever combine to form a dynamic PV module, which is then mounted on a cable net supporting structure. An exploded view of these components can be seen in Figure 5.3. There are also additional electronics which exists off the facade in a separate control box. These five components along with the assembly, are the main product systems in the manufacture of an ASF as seen in Figure 5.4. The inventory quantities are given in specific mass quantity (SMQ), which is the mass in kg of the specific materials.

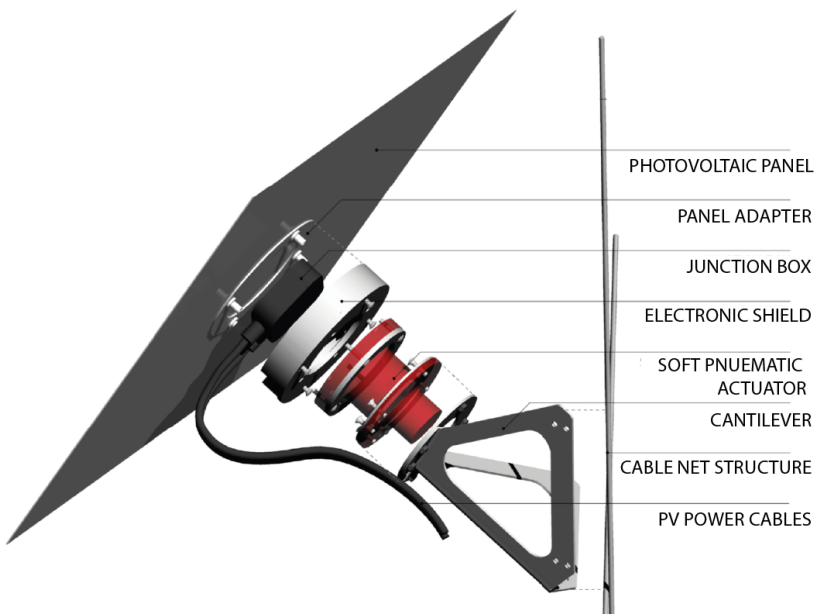


FIGURE 5.3: Exploded view of an ASF module mounted on a cable net supporting structure

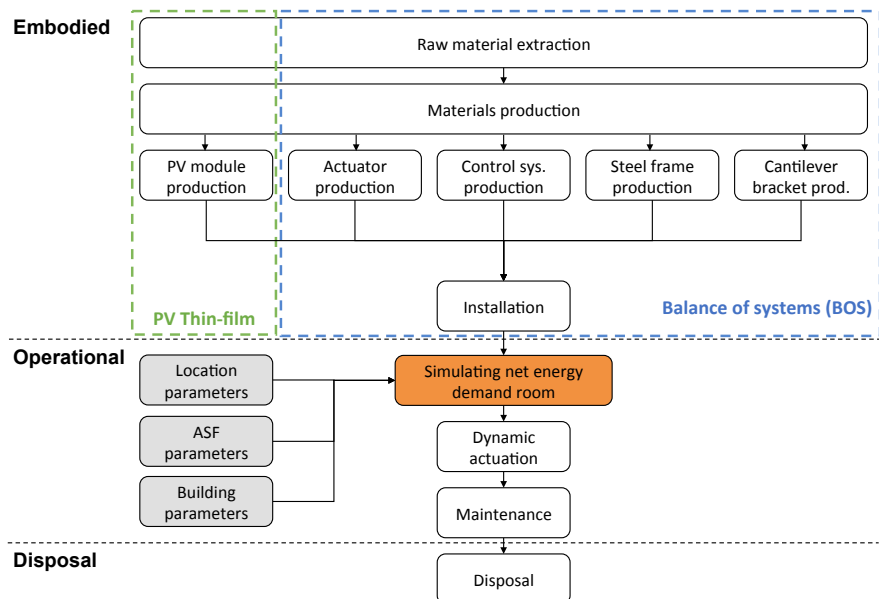


FIGURE 5.4: Breakdown of the ASF into five embodied product components, installation, operation, and disposal

PV PANEL

Weight is the primary restriction when selecting a PV panel. Any technology that requires glass encapsulation or a heavy substructure can therefore not be used. The technology also needs to be on the market with high module efficiency. CIGS PV panels were selected as the thin film panel of choice due to its high efficiency, low cost, and ability to be deposited on a polymer or aluminium substrate [81].

Material description	SMQ
CIGS PV film	$0.569 \text{ m}_{\text{PV}}^2 / \text{m}_{\text{facade}}^2$
Aluminum sheet	$1.593 \text{ kg/m}_{\text{facade}}^2$
Chromium steel panel adapter	$1.422 \text{ kg/m}_{\text{facade}}^2$
Polyethylene for junction box	$0.036 \text{ kg/m}_{\text{facade}}^2$
Diode, glass for junction box	$0.011 \text{ kg/m}_{\text{facade}}^2$

TABLE 5.1: Inventory in specific mass quantity (SMQ) of the top five input flows to the PV manufacturing process

ACTUATOR

Traditionally photovoltaic actuation is done through the use of servo motors. Servo motors however become a limiting factor for adaptive facades due to their high upfront costs, and instability in heavy winds. Soft robotic actuators on the other hand are cheaper and more resilient to harsh environmental conditions [82]. The soft robotic actuators however are still in development and have an estimated lifetime of five years. They will therefore require three rounds of maintenance during the lifetime of the ASF. For the purpose of this assessment we will run a sensitivity analysis on the use of servo motors and soft robotic actuators.

Material description	SMQ
Chromium steel rings	$1.0665 \text{ kg/m}_{\text{facade}}^2$
Electronics, for control, 2-way valves	$0.0130 \text{ kg/m}_{\text{facade}}^2$
Silicone chambers	$0.8887 \text{ kg/m}_{\text{facade}}^2$
Polyurethane tubes	$0.0933 \text{ kg/m}_{\text{facade}}^2$
Air compressor, screw type, 0.75kW	$1.7281 \text{ kg/m}_{\text{facade}}^2$

TABLE 5.2: Inventory of four main input flows to the soft robotic actuator manufacturing process

CANTILEVER

The cantilever is a steel connection point between the PV panel and the supporting structure.

Material description	SMQ
Chromium steel bracket	1.4220 kg/m ² _{facade}
Chromium steel fixing clamp	0.0284 kg/m ² _{facade}

TABLE 5.3: Inventory of main input flows to the cantilever manufacturing process

SUPPORTING STRUCTURE

The supporting structure is the connection point between the array of photovoltaic modules and the building itself. Many different designs are possible, however, we will base our analysis of an existing adaptive solar facade [7]. This design consists of a steel cable-net that spans a steel supporting frame. The steel frame is then mounted on the building facade.

Material description	SMQ
Chromium steel frame	6.9928 kg/m ² _{facade}
Chromium steel swaged external thread	0.2897 kg/m ² _{facade}
Chromium steel wire rope WC	0.1593 kg/m ² _{facade}

TABLE 5.4: Inventory of the four main input flows to the manufacturing process of the Supporting Structure

CONTROL SYSTEM AND ELECTRONICS

The control system is required for the actuation of panels and the regulation of photovoltaic electricity production.

Material description	SMQ
Inverter 1.25kW	0.6090 kg/m ² _{facade}
PV cable	0.256 kg/m ² _{facade}
Control Electronics	0.0516 kg/m ² _{facade}

TABLE 5.5: Inventory of the four main input flows to the manufacturing process of the Control System

ASSEMBLY

There are many assembly options available. From past experience,

an installation of an equivalent ASF required a hydraulic hoist which was in operation for eight hours [71].

Material description	SMQ
Hoist, diesel <18.64kW, idling	0.5267 h/m ² _{Facade}

TABLE 5.6: Inventory of main input flows to the Assembly Process

5.2.2 *Operational Life Cycle Inventory*

The operational inventory is categorised as 1) energy consumption of an office room 2) electricity consumption through dynamic actuation, and 3) maintenance.

BUILDING ENERGY CONSUMPTION:

An adaptive shading system, when mounted over a glazed facade, has an impact on the energy consumption of the building. More specifically, it has an impact on the heating cooling and lighting loads as described in Section 5.1. Previously conducted simulations compared three scenarios: 1) facade with no shading, 2) a facade with a static shading system, optimally angled at 45° to the horizontal axis, and 3) an adaptive solar facade [71].

The simulation was conducted on a south facing office room. The room, 7.0 meters in length, 4.9 meters wide and 3.1 meters high was modeled using Rhinoceros 3D CAD Package [19]. Grasshopper [20] was used to model the orientation of each photovoltaic panel. The geometrical input is imported to Energy Plus [83] through the DIVA [84] interface. A single zone thermal analysis was conducted for each possible geometrical configuration of the ASF for each hour of the year. The results were then post processed in MATLAB [85].

The simulations show a total energy saving of 25% compared to static panels at 45° and 56% compared to a case with no facade shading [71]. These results are summarised in Figure 5.5. This data is used to perform our previously described sensitivity analysis which also accounts for HVAC energy savings through adaptive shading.

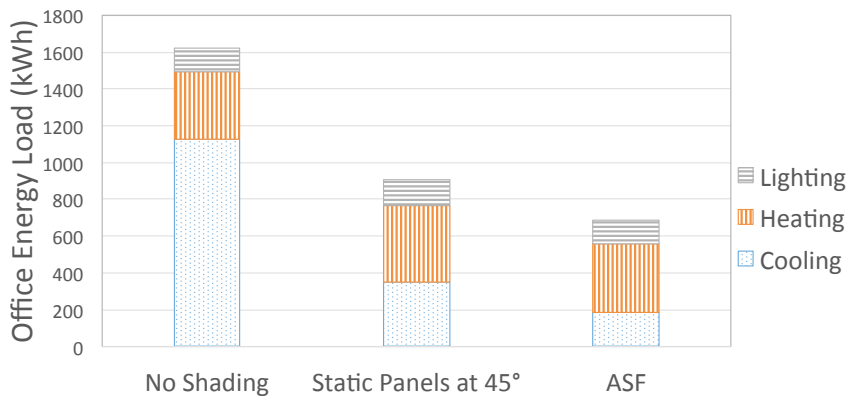


FIGURE 5.5: Breakdown of operational energy consumption for a system in Frankfurt am Main with a) no shading, b) with louvers at 45° and c) with an ASF – not including onsite electricity production.

DYNAMIC ACTUATION: The energy required for actuation is also taken into account. It takes 0.31Wh to fully open a single actuator. Based on the assumption of four full openings and closings per day per actuator, we approximate the combined energy requirement to be 489kWh in its 20 year lifetime.

MAINTENANCE: Soft robotic actuators currently have a lifetime of five years, and therefore will need to be replaced three times during the 20 year lifetime of an ASF. No other maintenance efforts are considered for the assessment of 20 years.

Building Settings

Office Envelope	Roof: Adiabatic Floor: Adiabatic Walls: Adiabatic
Thermal Set Points	Window: Double Glazed ($e=0.2$) 3mm/13mm air Heating: 22°C Cooling: 26°C
Building System	Hydronic Heating: COP=4 Hydronic Cooling: COP=3
Lighting Control	Lighting Load: 11.8W/m ² Lighting Control: 300 lx Threshold
Occupancy	Office: Weekdays from 8:00-18:00 People set point: 0.1 persons/m ² Infiltration: 0.5 air changes per hour

Location Assumptions

Weather File	Frankfurt am Main, Germany (106370IWEC)
Electricity Mix	Germany (DE) [86]
Average Solar Radiation	855kWh/m ² /year

Maintenance

Actuator Changes	Every 5 years
------------------	---------------

ASF Assumptions

Full openings and closings	4 per day
----------------------------	-----------

TABLE 5.7: Summary of main assumptions for the calculation of operational emissions

5.2.3 Sensitivity Analysis

In order to evaluate the impact of varying parameters on the LCA, we performed a sensitivity analysis on the following assumptions

- When an ASF is built over a glazed building surface, thus including the effects of adaptive shading on the building energy consumption.
- The location of the ASF including the effects of the GWP of the local electricity mix. Assessments will also be run in Madrid and Geneva.
- A static version of the ASF, where panels are optimally orientated at 45° to the horizontal (altitude) axis.
- The type of actuation system (servo motors compared to soft robotic actuators).
- The complexity of the control system. The ASF can be built where each panel is independently actuated, or a case where it is actuated in rows. When the panels are actuated independently more valves and control electronics are required.

5.3 RESULTS

We present the results of the LCA analysis in relation to the 1) embodied emissions, 2) a calculation of the emission factor, 3) sensitivity of the LCA to design and location, and 4) a comparison to other PV technologies.

5.3.1 *LCA of the Adaptive Solar Facade Manufacture*

A breakdown of six major midpoint impact indicators based of the ReCiPe methodology [87] can be found in Figure 5.6. The largest embodied GWP contribution in the ASF comes from the solar panels, followed by the electronics and the supporting structure. The control and electronics systems play a large role in freshwater eutrophication, and human toxicity due to the high life cycle emissions of electronic systems.

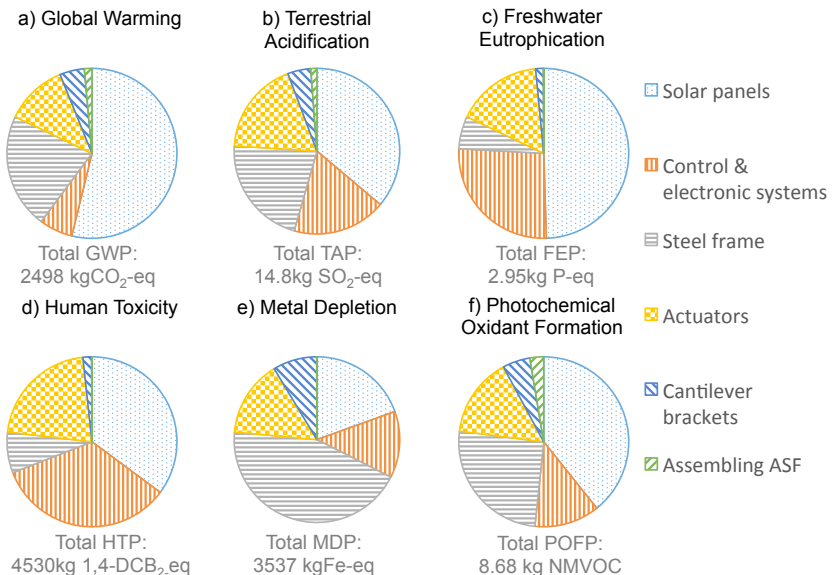


FIGURE 5.6: Embodied emission breakdown of six major midpoint indicators.
The solar panels, control/electronics, and steel frame have the highest life cycle impact

5.3.2 Calculation of GWP Emission Factor

The combined GWP of main inputs to the ASF, previously described in Figure 5.4, can be illustrated using a waterfall chart as shown in Figure 5.7.

This gives us a final emission of 3037 kgCO₂-eq. When we include the energy savings through adaptive shading in our system expansion, the final emissions come down to -8318 kgCO₂-eq. Dividing these values by the photovoltaic electricity production over a 20 year life time of 9175 kWh, we get an emission factor of 331 gCO₂-eq/kWh for the system without adaptive shading and -906 gCO₂-eq/kWh with adaptive shading.

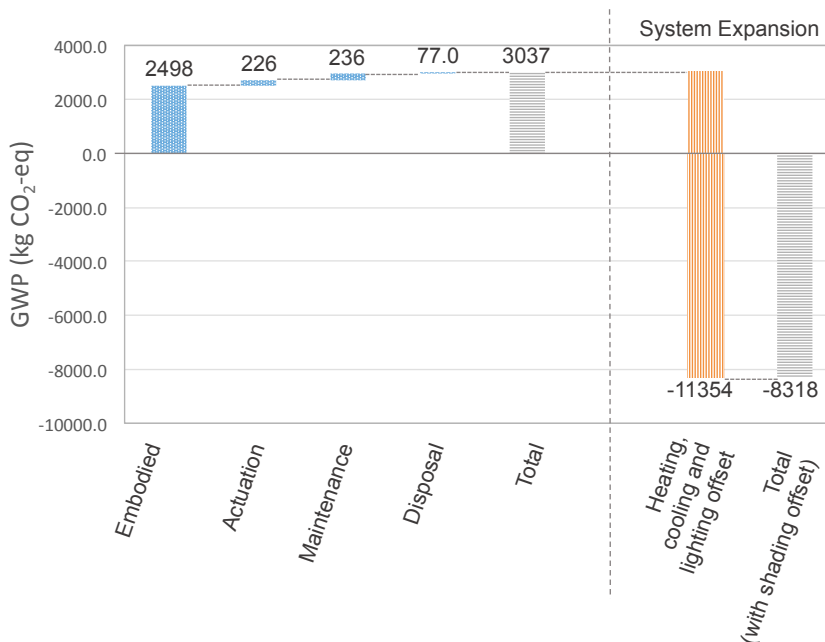


FIGURE 5.7: Waterfall diagram of GWP of the ASF not including photovoltaic electricity production. When reading from left to right, the far left bar details the embodied carbon emissions. The second, third and fourth bar detail the actuation, maintenance, and disposal respectively. This leaves us with our final emissions value (grey bar) of 3037kgCO₂-eq. The orange bar details the emission reduction through adaptive shading which is part of our system expansion bringing the total down to -8318kgCO₂-eq. When we divide these totals by the photovoltaic electricity production (9174kWh) we gain an emission factor of 331gCO₂-eq/kWh for the system without adaptive shading and -906 gCO₂-eq/kWh with adaptive shading. Note that the waterfall chart itself doesn't show PV electricity generation. This is taken into account in the emission factor.

5.3.3 Sensitivity Analysis

The sensitivity analysis is shown in Figure 5.8. The performance of the ASF is dependent on the location where it is operated as explained in Section 5.2.2. Changing the weather files of the simulation, and the electricity

mix of the country brings interesting results. Geneva has a similar climate to Frankfurt, however the local electricity mix is dominated by hydro and nuclear power which has a very low GWP potential [86]. This would then increase the emission factor of the ASF to 53.5 gCO₂-eq/kWh. This difference arises as the greenhouse gas emission savings of adaptive shading are dependent on the emission factor of the grid mix. Spain on the other hand has a warmer climate, with higher solar radiation, but a less greenhouse gas intensive electricity mix. This ultimately results in a similar emission factor of the ASF of -825 gCO₂-eq/kWh.

We also present a case where we remove the actuators and necessary control system for a dynamic system. Instead, we have panels that are optimally orientated at 45° to the horizontal axis. This reduces embodied greenhouse gas emissions by 12.1% from the baseline highlighted in Figure 5.6. However the reduction in electricity production, and savings through adaptive shading, result in a 15% higher emission factor.

The choice of actuator has a small impact on the embodied carbon emissions. Changing a single Soft Robotic Actuator (including the air compressor, tubing, and maintenance) to a classical servo motor increases the total embodied GWP by 23% from 2498 kg CO₂-eq to 3073 kg CO₂-eq. However, the servo motors have lower operational emissions and maintenance. Ultimately an ASF with servo motors has a 1.5% higher emission factor.

The control system design should be carefully thought out due to the high embodied human toxicity, freshwater eutrophication and terrestrial acidification. However simplifying the actuation control electronics has a minimal effect as the majority of the emissions lie in the inverter, cables, and air compressor. In terms of GWP, there is a 0.3% difference which is negligible.

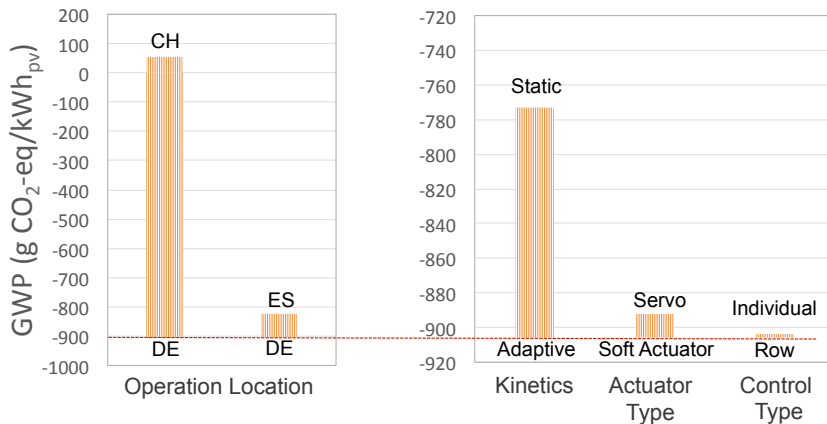


FIGURE 5.8: Sensitivity analysis of the emission factor including the HVAC impact of adaptive shading based on location, actuation system, and control system

5.3.4 Comparison to existing PV technologies

Comparison of the ASF to other PV technologies and the German electricity mix is highlighted in Figure 5.9. This comparison is conducted in Frankfurt am Main with an average irradiation of $855 \text{ kWh/m}^2/\text{year}$.

The blue bars detail systems with no added shading benefits. Here we present the ASF, a static optimally orientated facade as used in Figure 5.8, and three classical flat facade installations. The orange bars detail the system expansion where the ASF is built over glazed surfaces which also bring energy savings to the building. Because the GWP savings through adaptive shading offsets the entire embodied GWP, we have a system with a negative emission factor.

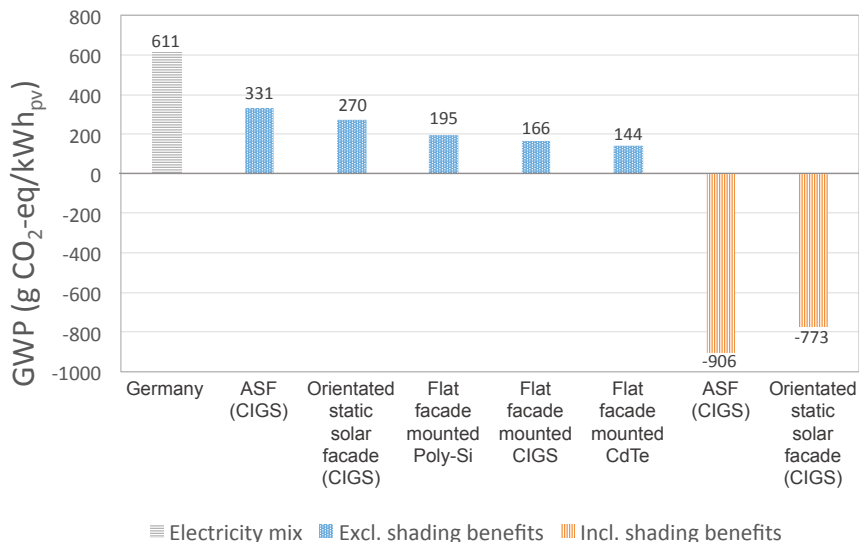


FIGURE 5.9: Comparison of facade installations in Germany with an average facade irradiation of 855kWh/m²/year. We compare an ASF to an optimally orientated static facade, and classic flat facade mounted PV solutions. The orange bars include the system expansion of energy savings through adaptive shading.

5.4 DISCUSSION

An adaptive solar facade, purely as a solar tracking and electricity generation technology is inferior to simple flat mounted static solutions in terms of life cycle emissions. Classic static facade mounted Poly-Si and CIGS solutions perform 40% to 50% better than the ASF respectively. This is due to the additional greenhouse gas emissions, caused by the material required for the control system, supporting structure, actuators, and the energy required for actuation. A static ASF where the solar panels are orientated for optimal harvest also has a lower life cycle performance compared to classic facade systems. This is because the added structure required for optimal orientation is not compensated by the added gains in photovoltaic production.

However when we also consider the multi functionality of the ASF and account for energy savings to the building through adaptive shading, we have a system that yields a negative emission factor of -906 gCO₂-eq/kWh. This is because the savings to the building system in terms of heating, cooling, and lighting offsets the embodied GWP four-fold. This demonstrates the advantage of using the PV material, not only as an electricity generation unit, but also as a building material for adaptive shading systems. In this analysis we also present a static ASF where all panels were orientated at an optimal angle of 45° to the horizontal axis. Although this solution performs well, it sacrifices user comfort. The users can not open the facade to suit their desires.

GWP savings through adaptive shading however are sensitive to the GWP of the electricity mix. A country with a low GWP electricity mix will result in lower operational GWP savings than a country with a high GWP electricity mix. For example, an ASF installed in Switzerland has a higher emission factor of 53.5 gCO₂-eq/kWh.

Although it is favorable to install an ASF in Germany, it still has benefits in countries such as Switzerland. For instance, with an emission factor 53% less than the standard mix, it contributes to a nuclear free energy mix. Furthermore, it provides interesting design options for architects where they can install PV in locations which were previously not possible. Thus increasing BIPV potential.

When designing an ASF architects and engineers may consider:

- The added benefit of a highly adaptable shading element
- The trade-off between soft robotic actuators and servo motors for actuation. Although the investigated soft robotic actuator has an embodied GWP three times lower than a servo motor, it requires three times more energy to actuate. Purely from an LCA perspective, if more than 6 actuations are required a day, servo motors would be the preferred solution.
- Control system electronics cost 27.5kgCO₂-eq/kg and play a large contribution in human toxicity, freshwater eutrophication and terrestrial acidification. They should therefore be carefully designed. However increasing the resolution of the ASF control system to allow each

panel to be independently actuated only increases the emission factor by 1.6gCO₂-eq/kWh.

- The structural support system in our current analysis used a stainless steel frame representing 22% of our total embodied carbon emissions, 21% of terrestrial acidification, 44% of metal depletion, and 25% of photochemical oxidant formation. Redesigning the frame to use less stainless steel, or an alternative material with a lower life cycle impact, such as plain steel, should be considered.
- If the ASF is installed in front of an opaque building surface then the advantages of adaptive shading are not present. In this case, a static, flat mounted system is a preferred design choice.

One limitation of the LCA is that the analysis focuses on a single office room. Expanding the analysis to the entire building, or urban level may yield different results. The LCA also assumes that the user will not override the system. In practice the facade will adapt to the desires of the user.

The LCA also excludes other aspects of building system such as the downsizing of heating and cooling appliances, the use of DC electricity on-site, and the increase in user comfort.

5.5 CONCLUSION

As an electricity producing device the ASF is outperformed by fixed PV systems. However it comes with the added benefit of building integration and multifunctionality, i.e. allowing for better control of solar loads and user comfort. When adding these aspects to the comparison (i.e. accounting for HVAC savings), the system becomes favourably competitive to a traditional PV system as it has a negative emission factor of -906gCO₂/kWh. These advantages however, will not be present if the ASF is installed over an opaque building surface. It is therefore preferable to install static systems over opaque facades, and keep the adaptive system for glazed facades only.

The design of an ASF can greatly influence the results. Varying factors such as the choice of actuators, the complexity of the control system, and the structural support can change the emission factor. The largest variable however is the emission factor of the grid electricity mix. The building operational savings in heating, cooling, and lighting will have a CO₂ saving based on the grid electricity mix.

Future research will validate the assumptions to building energy consumption through experimentation, and test the users response. This will be conducted on the ETH House of Natural Resources living lab where an example of an ASF has already been constructed [7]. Further numerical simulations of the ASF on different building typologies, building systems and climates will enable us to specifically target the best application scenario.

To conclude, we demonstrated that BIPV systems and adaptive shading elements complement each other successfully. We see an improvement in environmental performance of the PV technology, and create new architectural possibilities for the aesthetic integration of PV panels over glazed building surfaces, thus expanding BIPV potential.

6

CONCLUSION

This thesis presents a holistic analysis of adaptive photovoltaic envelopes from design and control, to evaluation. I first present the performative design environment for the fabrication of kinetic architectural elements. Here I show how the multiple fields of structural engineering, energy engineering, control engineering, industrial design, and architecture can be combined into a single automated workflow that accelerates the design process. I then present how the adaptive system can be controlled using a model predictive algorithm which combines building energy demand and solar radiation simulations. From the simulation outputs, the adaptive system can determine the best physical configuration to minimise the net energy building demand. This framework can be used, to not only control the facade, but to evaluate the energy saving potential of an adaptive photovoltaic envelope over a static system. Our results show that there is a 20% - 80% energy saving potential compared to an equivalent static system. The range of these results are large as they are heavily dependent on the building type. This framework is therefore run for 11 different building use types spanning six construction periods. Results show that the ASF performs best in environments where there is a mix of both heating and cooling demands. For buildings that predominantly have cooling demands, a simple static system at an optimum solar angle would be the most cost effective solutions. Likewise for a building that predominantly consists of heating demands, a window without shading, or a manually controlled Venetian blind may be optimal. The ASF performs best in modern offices, retail stores, food stores and schools. Finally, I extract the results of a modern office based simulation and conduct a CO₂ life cycle analysis. Results show that the ASF, running purely as an electricity producing device, is outperformed by static PV systems by 50%. However when I include the energy saving to the building interior, the ASF becomes favourably competitive to a traditional PV system.

6.1 OUTLOOK

So what does this mean for the future of adaptive architecture?

This question lies in the hands of future architects. In essence this thesis is a feasibility study that describes how an adaptive system can be designed, controlled and evaluated; using the adaptive solar facade as a case study. In reality, adaptive architecture will not just be limited to kinetic envelopes, but any technology that has the potential to vary its property. Examples could include walls with varying thermal resistances, or variable ventilation systems.

The kinetic envelope however, has a property that other adaptive technologies lack. And that is the architectural expression of the building. An adaptive facade evolves a building from a static system to one that feels alive and changes with variation in the season, the day, the weather, or its use.

One remaining step in this technology that hasn't been addressed in this thesis is the interaction with users. The users currently have the ability to override the adaptive algorithm in order to open or close the panels. This override, however, should also be integrated into a machine learning algorithm to enable the facade not just to adapt to the external conditions, but to the desires of the user. This research will be possible once the constructed ASF is installed on the HiLo building.

A

APPENDIX

A.1 FULL SET OF EQUATIONS TO THE BUILDING MODEL

The following equations are based on the ISO 13790 standard [25]. Denoting by T_m , the temperature of the thermal mass in the room,

$$T_m(H_{tr3} + H_e) + C_m \frac{dT_m}{dt} = \phi_{mtot} \quad (\text{A.1})$$

The value ϕ_{mtot} represents an equivalent thermal heat flux and is given by,

$$\phi_{mtot} = \phi_m + H_e T_e + \frac{H_{tr3}}{H_{tr2}} (\phi_{st} + H_w T_e + H_{tr1} T_{sup} + \frac{H_{tr1}}{H_{ve}} (\phi_{HC} + \phi_{io})) \quad (\text{A.2})$$

where C_m is the thermal capacitance of the room, T_e is the external air temperature, T_{sup} is the conditioned air supply temperature. The solar heat gains ϕ_{sol} , and internal heat gains ϕ_{int} are represented by three equivalent heat fluxes ϕ_{io} , ϕ_{st} and ϕ_m which correspond to a heat exchange to the air T_{air} , internal room surface T_s , and thermal mass T_m respectively. The heating and cooling heat flux is represented by ϕ_{HC} . The five thermal conductances H are represented by three equivalent conductances

$$H_{tr1} = \frac{1}{1/H_{ve} + 1/H_{is}} \quad (\text{A.3})$$

$$H_{tr2} = H_{tr1} + H_w \quad (\text{A.4})$$

$$H_{tr3} = \frac{1}{1/H_{tr2} + 1/H_{ms}} \quad (\text{A.5})$$

The internal heat flow rates due to internal gains and solar sources are divided between the thermal nodes by

$$\phi_{io} = 0.5\phi_{int} \quad (\text{A.6})$$

$$\phi_m = \frac{A_m}{A_t} (0.5\phi_{int} + \phi_{sol}) \quad (\text{A.7})$$

$$\phi_{st} = \left(1 - \frac{A_m}{A_t} - \frac{H_w}{9.1 * A_t}\right)(0.5\phi_{int} + \phi_{sol}) \quad (\text{A.8})$$

Applying the Crank-Nicolson method [62] to Equation 3.1 gives us the discrete differential equation:

$$T_{m_{k+1}} = \frac{\phi_{mtot} + T_{m_k}(\frac{C_m}{\Delta t} - 0.5(H_{tr3} + H_e))}{\frac{C_m}{\Delta t} + 0.5(H_{tr3} + H_e)} \quad (\text{A.9})$$

A.2 LCA PARAMETERS

A.2.1 Electricity production of different PV Systems

	ASF	Orientated Solar Facade	Flat CIGS	Flat CdTe	Flat PolySi
Total Irradiation (kWh/m ² /year)	855.0	855.0	855.0	855.0	855.0
Utility Factor (m ² /m ²)	0.69	0.69	0.69	0.69	0.69
Losses from sub optimal angle	0.00	0.30	0.38	0.38	0.38
Irradiation of active PV (kWh/m ² /year)	593.8	415.6	365.3	365.3	365.3
Efficiency	0.11	0.11	0.11	0.10	0.14
Self Shading Losses	0.40	0.40	0.00	0.00	0.00
Losses due to sub optimal tracking angle	0.77	1.00	1.00	1.00	1.00
Total Power (kWh/year)	458.7	417.0	610.8	555.3	777.4

TABLE A.1: Total PV production for the ASF, a static version of the ASF in an optimal orientation for building shading and PV production, and classical flat facade mounts of CIGS, CdTe and PolySi panels in Frankfurt, Germany

A.2.2 *Major Contributions to Disposal*

	GWP	TAP
Treatment of waste polyurethane, municipal incineration	32.7	0.0223
Treatment of waste electric wiring, collection for final disposal	31.6	0.0162
Treatment of scrap aluminium, municipal incineration	3.93	0.0404
Treatment of scrap steel, municipal incineration	3.7	0.039
Treatment of electronics scrap from control units	2.89	0.001
Treatment of waste polyethylene, municipal incineration	1.07	0.0001
Market for waste electric, and electronic equipment	0.923	0.00178
Treatment of scrap copper, municipal incineration	0.285	0.00051

TABLE A.2: Major Disposal Global Warming Potential (GWP) and Terrestrial Acidification Potential (TAP) contributions to the Disposal of an ASF. Note that the cut off system model is used.

BIBLIOGRAPHY

1. Mohr, P., Taylor, B. & Newell, D. 2014 CODATA Recommended Values of the Fundamental Physical Constants <http://physics.nist.gov/constants>. (Online; accessed 2015-11-26). 2015.
2. Klepeis, N. E., Nelson, W. C., Ott, W. R., Robinson, J. P., Tsang, A. M., Switzer, P., Behar, J. V., Hern, S. C. & Engelmann, W. H. The National Human Activity Pattern Survey (NHAPS): a resource for assessing exposure to environmental pollutants. *Journal of Exposure Science and Environmental Epidemiology* **11**, 231 (2001).
3. Fifth Assessment Report, Mitigation of Climate Change. *Intergovernmental Panel on Climate Change*, 674 (2014).
4. Oborn, P. *Al Bahr Towers: The Abu Dhabi Investment Council Headquarters* (John Wiley & Sons, 2012).
5. Block, P., Schlueter, A., Veenendaal, D., Bakker, J., Begle, M., Hofer, J., Jayathissa, P., Lydon, G., Maxwell, I., Mendez Echenagucia, T., Nagy, Z., Pigram, D., Svetozarevic, B., Torsing, R., Verbeek, J. & Willmann, A. NEST HiLo: Research & innovation unit for lightweight construction and building systems integration. *Journal of Building Engineering*. under review (2017).
6. Loonen, R., Trčka, M., Cóstola, D. & Hensen, J. Climate adaptive building shells: State-of-the-art and future challenges. *Renewable and Sustainable Energy Reviews* **25**, 483 (2013).
7. Nagy, Z., Svetozarevic, B., Jayathissa, P., Begle, M., Hofer, J., Lydon, G., Willmann, A. & Schlueter, A. The Adaptive Solar Facade: From concept to prototypes. *Frontiers of Architectural Research* **5**, 143 (2016).
8. Jayathissa, P., Luzzatto, M., Schmidli, J., Hofer, J., Nagy, Z. & Schlueter, A. Optimising building net energy demand with dynamic BIPV shading. *Applied Energy* **202**, 726 (2017).
9. Schlueter, A. & Thesseling, F. Building information model based energy / exergy performance assessment in early design stages. *Automation in construction* **18**, 153 (2009).

10. Volk, R., Stengel, J. & Schultmann, F. Building Information Modeling (BIM) for existing buildings Literature review and future needs. *Automation in construction* **38**, 109 (2014).
11. Oxman, R. Performance-based design: current practices and research issues. *International journal of architectural computing* **6**, 1 (2008).
12. Turrin, M., Von Buelow, P., Kilian, A. & Stouffs, R. Performative skins for passive climatic comfort: A parametric design process. *Automation in Construction* **22**, 36 (2012).
13. Rippmann, M., Lachauer, L. & Block, P. Interactive Vault Design. *International Journal of Space Structures* **27**, 219 (2012).
14. Holzer, D. Design exploration supported by digital tool ecologies. *Automation in Construction* **72**, 3 (2016).
15. Kim, D.-Y. & Kim, S.-A. An exploratory model on the usability of a prototyping-process for designing of Smart Building Envelopes. *Automation in Construction* (2017).
16. Diaz, H., Alarcon, L. F., Mourgués, C. & Garcia, S. Multidisciplinary design optimization through process integration in the AEC industry: Strategies and challenges. *Automation in Construction* **73**, 102 (2017).
17. Negendahl, K. Building performance simulation in the early design stage: An introduction to integrated dynamic models. *Automation in Construction* **54**, 39 (2015).
18. Lydon, G., Hofer, J., Svetozarevic, B., Nagy, Z. & Schlueter, A. Coupling energy systems with lightweight structures for a net plus energy building. *Applied Energy* **189**, 310 (2017).
19. Rhinoceros V5 <<https://www.rhino3d.com/>> (2015).
20. Grasshopper - Algorithmic Modelling for Rhino <<http://www.grasshopper3d.com/>> (2015).
21. Python <<https://www.python.org/>> (2017).
22. karamba 3d <<http://www.karamba3d.com/>> (2017).
23. Roudsari, M. S., Pak, M. & Smith, A. *Ladybug: a parametric environmental plugin for grasshopper to help designers create an environmentally-conscious design* in *Proceedings of the 13th International IBPSA Conference Held in Lyon, France Aug* (2013).
24. Hofer, J., Groenewolt, A., Jayathissa, P., Nagy, Z. & Schlueter, A. Parametric analysis and systems design of dynamic photovoltaic shading modules. *Energy Science & Engineering* **4**, 134 (2016).

25. EN ISO 13790: *Energy Performance of Buildings: Calculation of Energy Use for Space Heating and Cooling (ISO 13790: 2008)*. (CEN, 2008).
26. Szokolay, S. V. *Environmental Science Handbook* (The Construction Press, 1980).
27. Jayathissa, P., Luzzatto, M. & Schmidli, J. *ASF Simulation Framework* <<https://github.com/architecture-building-systems/ASF%5C-Simulation>> (2017).
28. Jayathissa, P. *RC Building Simulator* <https://github.com/architecture-building-systems/RC%5C_BuildingSimulator> (2017).
29. Svetozarevic, B., Schlueter, A., Hischier, I., Begle, M., Jayathissa, P., Caranovic, S., Shepherd, R., Nagy, Z. & Hofer, J. Soft robotics driven dynamic building envelope for energy and comfort management. *In Submission* (2017).
30. Svetozarevic, B., Nagy, Z., Hofer, J., Jacob, D., Begle, M., Chatzi, E. & Schlueter, A. *SoRo-Track: A two-axis soft robotic platform for solar tracking and building-integrated photovoltaic applications in Robotics and Automation (ICRA), 2016 IEEE International Conference on* (2016), 4945.
31. Defaix, P., van Sark, W., Worrell, E. & de Visser, E. Technical potential for photovoltaics on buildings in the EU-27. *Solar Energy* **86**, 2644 (2012).
32. Raugei, M. & Frankl, P. Life cycle impacts and costs of photovoltaic systems: current state of the art and future outlooks. *Energy* **34**, 392 (2009).
33. Wilson, G. *Cell Efficiency Records* <<http://www.nrel.gov/ncpv/>> (2015).
34. Kushiya, K. CIS-based thin-film PV technology in solar frontier KK. *Solar Energy Materials and Solar Cells* **122**, 309 (2014).
35. Kaelin, M., Rudmann, D. & Tiwari, A. Low cost processing of CIGS thin film solar cells. *Solar Energy* **77**, 749 (2004).
36. Jelle, B. P., Breivik, C. & Røkenes, H. D. Building integrated photovoltaic products: A state-of-the-art review and future research opportunities. *Solar Energy Materials and Solar Cells* **100**, 69 (2012).
37. Perez, M. J., Fthenakis, V., Kim, H.-C. & Pereira, A. O. Facade integrated photovoltaics: a life cycle and performance assessment case study. *Progress in Photovoltaics: Research and Applications* **20**, 975 (2012).

38. Jayathissa, P., Jansen, M., Heeren, N., Nagy, Z. & Schlueter, A. Life cycle assessment of dynamic building integrated photovoltaics. *Solar Energy Materials and Solar Cells* **156**, 75 (2016).
39. Li, D. H., Lam, T. N., Chan, W. W. & Mak, A. H. Energy and cost analysis of semi-transparent photovoltaic in office buildings. *Applied Energy* **86**, 722 (2009).
40. Peng, J., Curcija, D. C., Lu, L., Selkowitz, S. E., Yang, H. & Zhang, W. Numerical investigation of the energy saving potential of a semi-transparent photovoltaic double-skin facade in a cool-summer Mediterranean climate. *Applied Energy* **165**, 345 (2016).
41. Vats, K. & Tiwari, G. Energy and exergy analysis of a building integrated semitransparent photovoltaic thermal (BISPV) system. *Applied Energy* **96**, 409 (2012).
42. Chae, Y. T., Kim, J., Park, H. & Shin, B. Building energy performance evaluation of building integrated photovoltaic (BIPV) window with semi-transparent solar cells. *Applied Energy* **129**, 217 (2014).
43. Bellia, L., Marino, C., Minichiello, F. & Pedace, A. An overview on solar shading systems for buildings. *Energy Procedia* **62**, 309 (2014).
44. Palmero-Marrero, A. I. & Oliveira, A. C. Effect of louver shading devices on building energy requirements. *Applied Energy* **87**, 2040 (2010).
45. Nielsen, M. V., Svendsen, S. & Jensen, L. B. Quantifying the potential of automated dynamic solar shading in office buildings through integrated simulations of energy and daylight. *Solar Energy* **85**, 757 (2011).
46. Sara, F. & et al. Maximizing the Solar Photovoltaic Yield in Different Building Facade Layouts. *EU PVSEC* (2015) (2015).
47. Sun, L., Lu, L. & Yang, H. Optimum design of shading-type building integrated photovoltaic claddings with different surface azimuth angles. *Applied Energy* **90**, 233 (2012).
48. Mandalaki, M., Zervas, K., Tsoutsos, T. & Vazakas, A. Assessment of fixed shading devices with integrated PV for efficient energy use. *Solar Energy* **86**, 2561 (2012).
49. Hu, Z., He, W., Ji, J., Hu, D., Lv, S., Chen, H. & Shen, Z. Comparative study on the annual performance of three types of building integrated photovoltaic (BIPV) Trombe wall system. *Applied Energy* **194**, 81 (2017).

50. Chatzipanagi, A., Frontini, F. & Virtuani, A. BIPV-temp: A demonstrative Building Integrated Photovoltaic installation. *Applied Energy* **173**, 1 (2016).
51. Jayathissa, P., Schmidli, J., Hofer, J. & Schlueter, A. Energy Performance of PV Modules as Adaptive Building Shading Systems. *EU PVSEC 2016* (2016).
52. Feurer, T., Reinhard, P., Avancini, E., Bissig, B., Lockinger, J., Fuchs, P., Carron, R., Weiss, T. P., Perrenoud, J., Stutterheim, S., *et al.* Progress in thin film CIGS photovoltaics—Research and development, manufacturing, and applications. *Progress in Photovoltaics: Research and Applications* (2016).
53. Ward, G. J. *The RADIANCE lighting simulation and rendering system* in *Proceedings of the 21st annual conference on Computer graphics and interactive techniques* (1994), 459.
54. Robinson, D. & Stone, A. *Irradiation modelling made simple: the cumulative sky approach and its applications* in *PLEA conference* (2004), 19.
55. Perez, R., Seals, R. & Michalsky, J. All-weather model for sky luminance distribution preliminary configuration and validation. *Solar energy* **50**, 235 (1993).
56. Tregenza, P. Subdivision of the sky hemisphere for luminance measurements. *Lighting Research and Technology* **19**, 13 (1987).
57. Mermoud, A. & Lejeune, T. eng. in (Munich).
58. Skoplaki, E. & Palyvos, J. Operating temperature of photovoltaic modules: A survey of pertinent correlations. *Renewable Energy* **34**, 23 (2009).
59. Bacher, P. & Madsen, H. Identifying suitable models for the heat dynamics of buildings. *Energy and Buildings* **43**, 1511 (2011).
60. Sonderegger, R. Diagnostic tests determining the thermal response of a house. *Lawrence Berkeley National Laboratory* (2010).
61. Madsen, H. & Holst, J. Estimation of continuous-time models for the heat dynamics of a building. *Energy and Buildings* **22**, 67 (1995).
62. Crank, J. & Nicolson, P. *A practical method for numerical evaluation of solutions of partial differential equations of the heat-conduction type* in *Mathematical Proceedings of the Cambridge Philosophical Society* **43** (1947), 50.
63. Remund, J. & Kunz, S. *METEONORM: Global meteorological database for solar energy and applied climatology* (Meteotest, 1997).

64. Fonseca, J. A., Thomas, D., Mosteiro, M., Hsieh, S., Happel, G., Sreepathi, B., Elesawy, A., Shi, Z. & Schlueter, A. *City Energy Analyst* 2.2 <<https://doi.org/10.5281/zenodo.556165>> (2017).
65. Lorenzo, E., Narvarte, L. & Munoz, J. Tracking and back-tracking. *Progress in Photovoltaics: Research and Applications* **19**, 747 (2011).
66. Jayathissa, P., Luzzatto, M., Schmidli, J., Hofer, J., Nagy, Z. & Schlueter, A. Optimising Building Net Energy Demand with Dynamic BIPV Shading. *Under Review* (2017).
67. Fonseca, J. A., Nguyen, T.-A., Schlueter, A. & Marechal, F. City Energy Analyst (CEA): Integrated framework for analysis and optimization of building energy systems in neighborhoods and city districts. *Energy and Buildings* **113**, 202 (2016).
68. Data, C. *Zurich Classification* <<https://en.climate-data.org/region/1174/>>.
69. Fonseca, J. *Archetype Properties from the CEA Toolbox* <<https://github.com/architecture-building-systems/CEAforArcGIS/tree/master/cea/databases/CH/Archetypes>> (2017).
70. Rossi, D., Nagy, Z. & Schlueter, A. Adaptive distributed robotics for environmental performance, occupant comfort and architectural expression. *International Journal of Architectural Computing* **10**, 341 (2012).
71. Jayathissa, P., Nagy, Z., Offedu, N. & Schlueter, A. Numerical Simulation of Energy Performance and Construction of the Adaptive Solar Facade. *Proceedings of the Advanced Building Skins* **2**, 52 (2015).
72. Raugei, M., Bargigli, S. & Ulgiati, S. Life cycle assessment and energy pay-back time of advanced photovoltaic modules: CdTe and CIS compared to poly-Si. *Energy* **32**, 1310 (2007).
73. De Wild-Scholten, M. M. Energy payback time and carbon footprint of commercial photovoltaic systems. *Solar Energy Materials and Solar Cells* **119**, 296 (2013).
74. Fthenakis, V. & Kim, H. C. Photovoltaics: Life-cycle analyses. *Solar Energy* **85**, 1609 (2011).
75. Mason, J., Fthenakis, V., Hansen, T. & Kim, H. Energy payback and life-cycle CO₂ emissions of the BOS in an optimized 3.5 MW PV installation. *Progress in Photovoltaics: Research and Applications* **14**, 179 (2006).

76. Finkbeiner, M., Inaba, A., Tan, R., Christiansen, K. & Kluppel, H.-J. The new international standards for life cycle assessment: ISO 14040 and ISO 14044. *The international journal of life cycle assessment* **11**, 80 (2006).
77. Ortiz, O., Castells, F. & Sonnemann, G. Sustainability in the construction industry: A review of recent developments based on LCA. *Construction and Building Materials* **23**, 28 (2009).
78. Frischknecht, R., Jungbluth, N., Althaus, H.-J., Doka, G., Dones, R., Heck, T., Hellweg, S., Hischier, R., Nemecek, T., Rebitzer, G., et al. The ecoinvent database: Overview and methodological framework (7 pp). *The international journal of life cycle assessment* **10**, 3 (2005).
79. Solomon, S. *Climate change 2007-the physical science basis: Working group I contribution to the fourth assessment report of the IPCC* (Cambridge University Press, 2007).
80. Ciroth, A. ICT for environment in life cycle applications openLCA new open source software for life cycle assessment. *The International Journal of Life Cycle Assessment* **12**, 209 (2007).
81. Chiril, A., Buecheler, S., Pianezzi, F., Bloesch, P., Gretener, C., Uhl, A. R., Fella, C., Kranz, L., Perrenoud, J., Seyrling, S., et al. Highly efficient Cu (In, Ga) Se₂ solar cells grown on flexible polymer films. *Nature materials* **10**, 857 (2011).
82. Svetozarevic, B., Nagy, Z., Rossi, D. & Schlueter, A. Experimental Characterization of a 2-DOF Soft Robotic Platform for Architectural Applications. *Robotics: Science and Systems, Workshop on Advances on Soft Robotics*, 2 (2014).
83. Crawley, D. B., Lawrie, L. K., Pedersen, C. O. & Winkelmann, F. C. Energy plus: energy simulation program. *ASHRAE journal* **42**, 49 (2000).
84. DIVA for Rhino <<http://diva4rhino.com/>> (2015).
85. MATLAB 2014b, *The MathWorks, Inc., Natick, Massachusetts, United States*.
86. Itten, R., Frischknecht, R. & Stucki, M. *Life cycle inventories of electricity mixes and grid 2012*.
87. Goedkoop, M., Heijungs, R., Huijbregts, M., De Schryver, A., Struijs, J. & van Zelm, R. ReCiPe 2008. *A life cycle impact assessment method which comprises harmonised category indicators at the midpoint and the endpoint level* **1** (2009).

CURRICULUM VITAE

PERSONAL DATA

Name	Prageeth Jayathissa
Date of Birth	September 28, 1988
Place of Birth	Melbourne, Australia
Citizen of	New Zealand

EDUCATION

2007 – 2010	University of Canterbury, Christchurch, New Zealand <i>Degree: BEng Bachelor of Mechanical Engineering</i>
2011 – 2014	ETH Zurich Zurich, Switzerland <i>Degree: Msc Master of Energy Science</i>

EXPERIENCE

2014 – 2017	Facade Engineer <i>HiLo Building, ETH Zurich,</i> Zurich, Switzerland
2014 –	Swiss Coordinator <i>Action from Switzerland,</i> Zurich, Switzerland
2010 – 2012	Co-Founder <i>PJDobbie Engineering,</i> Christchurch, New Zealand

PUBLICATIONS

Articles in peer-reviewed journals:

1. Jayathissa, P., Caranovic, S., Hofer, J., Nagy, Z. & Schlueter, A. Parametric Design Environment for Kinetic Photovoltaic Architecture. *In Production* (2017).
2. Jayathissa, P., Luzzatto, M., Schmidl, J., Hofer, J., Nagy, Z. & Schlueter, A. Optimising Building Net Energy Demand with Dynamic BIPV shading. *Applied Energy* (2017).
3. Jayathissa, P., Jansen, M., Heeren, N., Nagy, Z. & Schlueter, A. Life cycle assessment of dynamic building integrated photovoltaics. *Solar Energy Materials and Solar Cells* **156**, 75 (2016).

Conference contributions:

4. Jayathissa, P., Zarb, J., Hofer, J. & Schlueter, A. *Sensitivity of Building Properties and Use Types for the Application of Adaptive Photovoltaic Shading Systems* in (Energy Procedia, 2017).
5. Jayathissa, P., Nagy, Z., Offedu, N. & Schlueter, A. *Numerical Simulation of Energy Performance and Construction of the Adaptive Solar Facade* in. **2** (TU Graz, 2015), 52.
6. Jayathissa, P., Schmidli, J., Hofer, J. & Schlueter, A. *Energy Performance of PV Modules as Adaptive Building Shading Systems* in (PVSEC, 2016).
7. Jayathissa, P., Caranovic, S., Begle, M., Svetozarevic, B., Hofer, J., Nagy, Z. & Schlueter, A. *Structural and Architectural Integration of Adaptive Photovoltaic Modules* in (ABS Bern, 2016).